



1 Reconstruction of the 1941 GLOF process chain at Lake Palcacocha (Cor- 2 dillera Blanca, Perú)

3 *Martin Mergili*^{1,2}, *Shiva P. Pudasaini*³, *Adam Emmer*⁴, *Jan-Thomas Fischer*⁵, *Alejo Co-*
4 *chachin*⁶, and *Holger Frey*⁷

5 ¹ Institute of Applied Geology, University of Natural Resources and Life Sciences (BOKU), Peter-Jordan-Straße 82,
6 1190 Vienna, Austria

7 ² Geomorphological Systems and Risk Research, Department of Geography and Regional Research, University of Vi-
8 enna, Universitätsstraße 7, 1010 Vienna, Austria

9 ³ Geophysics Section, Institute of Geosciences and Meteorology, University of Bonn, Meckenheimer Allee 176, 53115
10 Bonn, Germany

11 ⁴ Department of the Human Dimensions of Global Change, Global Change Research Institute, The Czech Academy of
12 Sciences, Bělidla 986/4a, 603 00, Brno, Czech Republic

13 ⁵ Department of Natural Hazards, Austrian Research Centre for Forests (BFW), Rennweg 1, 6020 Innsbruck, Austria

14 ⁶ Unidad de Glaciología y Recursos Hídricos, Autoridad Nacional del Agua, Confraternidad Internacional 167, Huaráz,
15 Perú

16 ⁷ Department of Geography, University of Zurich, Winterthurerstrasse 190, 8057 Zurich, Switzerland

17 Correspondence to: M. Mergili (martin.mergili@boku.ac.at)

18 Abstract

19 The Cordillera Blanca in Perú has been the scene of rapid deglaciation for many decades. One of numerous lakes
20 formed in the front of the retreating glaciers is the moraine-dammed Lake Palcacocha, which drained suddenly due to
21 an unknown cause in 1941. The resulting Glacial Lake Outburst Flood (GLOF) led to dam failure and complete drain-
22 age of Lake Jircacocha downstream, and to major destruction and thousands of fatalities in the city of Huaráz at a dis-
23 tance of 23 km. Lake Palcacocha has dramatically regrown through further glacial retreat since then and nowadays is
24 again considered a threat to the downstream communities. Previously, various types of computer simulations were
25 carried out in order to quantify the possible impact of future GLOFs from Lake Palcacocha, but no attempts are made
26 yet to back-calculate the 1941 event. Here, we chose an integrated approach to revisit the 1941 event in terms of topo-
27 graphic reconstruction and numerical back-calculation with the GIS-based open source mass flow/process chain simu-
28 lation framework r.avaflow. Thereby we consider four scenarios: (A) and (AX) breach of the moraine dam of Lake
29 Palcacocha due to retrogressive erosion, assuming two different fluid characteristics; (B) failure of the moraine dam
30 caused by the impact of a landslide onto the lake; and (C) geomechanical failure and collapse of the moraine dam. The
31 simulations largely yield empirically adequate results with physically plausible parameters, taking the documentation
32 of the 1941 event and previous calculations of future scenarios as reference. The results of the scenarios indicate that
33 the most likely initiation mechanism would be retrogressive erosion, possibly triggered by a minor impact wave
34 and/or facilitated by a weak stability condition of the moraine dam. However, the involvement of Lake Jircacocha
35 disguises part of the signal of process initiation farther downstream.

36 Keywords: GLOF, high-mountain lakes, Lake Palcacocha, numerical simulation, process chain, r.avaflow, two-phase
37 flows



38 1 Introduction

39 Glacial retreat in high-mountain areas often leads, after some lag time (Harrison et al., 2018), to the formation of pro-
40 glacial lakes, which are impounded by moraine dams or bedrock swells. Such lakes may drain suddenly, releasing a
41 large amount of water which may result in complex and potentially catastrophic process chains downstream. Glacial
42 lakes and outburst floods (GLOFs) have been subject of numerous studies covering many mountain regions all around
43 the globe (Hewitt, 1982; Haeberli, 1983; Richardson and Reynolds, 2000; Huggel et al., 2003; Breien et al., 2008;
44 Hewitt and Liu, 2010; Bolch et al., 2011; Mergili and Schneider, 2011; Mergili et al., 2013; Clague and O'Connor, 2014;
45 Emmer et al., 2015, 2016).

46 The Cordillera Blanca (Perú) represents the most glacierized mountain chain of the Tropics. Glacial lakes and GLOFs
47 are particularly common there (Carey, 2005). 882 high-mountain lakes were identified by Emmer et al. (2016). Some
48 of these lakes are susceptible to GLOFs (Vilímek et al., 2005; Emmer and Vilímek, 2013, 2014; ANA, 2014; Iturrizaga,
49 2014). A total of 28 geomorphologically effective GLOFs originating from moraine-dammed lakes have been docu-
50 mented (Emmer, 2017). Most recently, GLOFs were recorded at Lake Safuna Alta (2002 – the trigger was a rock ava-
51 lanche into the lake; Hubbard et al., 2005), at Lake Palcacocha (2003 – landslide-induced overtopping of the dam;
52 Vilímek et al., 2005), and at Lake 513 (2010 – triggered by an ice avalanche; Carey et al., 2012). Lake Artizón Alto was
53 hit by a landslide from a moraine in 2012, which resulted in cascading effects involving three more lakes and entrain-
54 ment of a considerable amount of debris in the Artizón Valley and, farther downstream, the Santa Cruz Valley
55 (Mergili et al., 2018a). A pronounced peak in frequency of high-magnitude GLOFs, however, was already observed in
56 the 1940s and 1950s, when lakes of notable size had formed behind steep terminal moraine walls (Emmer et al., 2019).
57 The most prominent and well-documented GLOF in this period occurred on 13 December 1941, when Lake Palcaco-
58 cha in the Quilcay Catchment drained suddenly, leading to a process chain that resulted in at least 1600 fatalities and
59 major destruction in the town of Huaráz 23 km downstream (Broggi, 1942; Oppenheim, 1946; Concha, 1952; Wegner,
60 2014).

61 In the Cordillera Blanca, the local population is highly vulnerable to high-mountain process chains, often induced by
62 GLOFs (Carey, 2005; Hofflinger et al., 2019). In order to mitigate this threat, tens of lakes in the Cordillera Blanca
63 have been remediated through technical measures such as open cuts, artificial dams or tunnels during the last decades
64 (Oppenheim, 1946; Zapata 1978; Portocarrero, 1984; Carey, 2005; Portocarrero, 2014; Emmer et al., 2018). However,
65 the management of GLOF risk is a difficult task (Carey et al., 2014). Anticipation of GLOF cascades – and, as a conse-
66 quence, also hazard mapping – relies to a large extent on the application of computational mass flow models (GAP-
67 HAZ, 2017). Important progress was made since the mid-20th Century: various models were developed, and have more
68 recently been implemented in simulation software tools (Voellmy, 1955; Savage and Hutter, 1989; Iverson, 1997;
69 Takahashi et al., 2002; Pitman and Le, 2005; McDougall and Hungr, 2004; Pudasaini and Hutter, 2007; Chisolm and
70 McKinney, 2018). Most of these approaches represent single-phase mixture models. Tools like RAMMS (Chris-
71 ten et al., 2010) or FLO-2D were used for the simulation of GLOFs (Mergili et al., 2011). Schneider et al. (2014),
72 Worni et al. (2014), and Somos-Valenzuela et al. (2016) have sequentially coupled two or more tools for simulating
73 landslide – GLOF cascades. However, single-phase models do not describe the interactions between the solid and the
74 fluid phase, or dynamic landslide-lake interactions, in an appropriate way, so that workarounds are necessary
75 (Gabl et al., 2015). Worni et al. (2014) called for integrated approaches. They would have to build on two- or even
76 three-phase models considering water, debris, and ice separately, but also the interactions between the phases and the
77 flow transformations. Pudasaini (2012) introduced a general two-phase flow model considering mixtures of solid parti-
78 cles and viscous fluid which has been used for the simulation of computer-generated examples of sub-aqueous land-
79 slides and particle transport (Kafle et al., 2016, 2019) as well as GLOFs (Kattel et al., 2016).



80 The recently introduced open source GIS simulation framework *r.avaflow* (Mergili et al., 2017) applies an extended
81 version of the approach of Pudasaini (2012). It was used to back-calculate the 2012 Santa Cruz process chain involving
82 four lakes (Mergili et al., 2018a), and the 1962 and 1970 Huascarán landslides (Mergili et al., 2018b), both in the Cor-
83 dillera Blanca. These studies identified the capability of that tool to appropriately simulate the transformations at the
84 boundary of individual processes, where one process transforms to the next, as one of the major challenges. Open is-
85 sues include the proper understanding of wave generation as a response to landslides impacting high-mountain lakes
86 and, as a consequence, the quantification of essential parameters such as the volume of overtopping water and the
87 discharge (Westoby et al., 2014). Further, uncertainties in the model parameters and the initial conditions accumulate
88 at process boundaries (Schaub et al. 2016), and threshold effects are expected to result in strongly non-linear responses
89 of the model error (Mergili et al., 2018a, b). In high-energy mass flows, the physical characteristics of the processes
90 involved are not always understood at the required level of detail (Mergili et al., 2018b).

91 On the one hand, flow models and simulation tools can help us to better understand some of the key mechanisms of
92 high-mountain process chains. On the other hand, well documented case studies are important to gain a better under-
93 standing on which questions can be tackled with simulation tools, and which questions cannot be answered without
94 further research. In the present work, we explore this field of uncertainty by applying the *r.avaflow* computational
95 tool to the 1941 Lake Palcacocha GLOF process chain. Thereby, based on the simulation of different scenarios, we
96 investigate on the following research questions:

- 97 1. What is the most likely release mechanism of initiating the process chain of the 1941 GLOF of Lake Palcac-
98 cha?
- 99 2. Are we able to back-calculate this process chain in an empirically adequate way with physically plausible
100 model parameters? Mergili et al. (2018b) reported a trade-off between these two criteria for the simulation of
101 the 1970 Huascarán landslide.
- 102 3. What are the major challenges in achieving successful (empirically adequate and physically plausible) simula-
103 tions?
- 104 4. What can we learn with regard to forward calculations of possible future events?

105 In Sect. 2 we depict the local conditions and the documentation of the event. After having introduced the computa-
106 tional framework *r.avaflow* (Sect. 3), we describe in detail the simulation input (Sect. 4) and our findings (Sect. 5). We
107 discuss the results (Sect. 6) and finally summarize the key points of the research (Sect. 7).

108 2 Lake Palcacocha

109 2.1 Quilcay catchment and Cojup Valley

110 Lake Palcacocha is part of a proglacial system in the headwaters of the Cojup Valley in the Cordillera Blanca, Perú
111 (Fig. 1). This system was – and is still – shaped by the glaciers originating from the southwestern slopes of Nevado
112 Palcaraju (6,264 m a.s.l.) and Nevado Pucaranra (6,156 m a.s.l.). A prominent horseshoe-shaped ridge of lateral and
113 terminal moraines marks the extent of the glacier during the first peak of the Little Ice Age, dated using lichenometry
114 to the 17th Century (Emmer, 2017). With glacier retreat, the depression behind the moraine ridge was filled with a
115 lake, named Lake Palcacocha. A photograph taken by Hans Kinzl in 1939 (Kinzl and Schneider, 1950) indicates a lake
116 level of 4,610 m a.s.l., allowing surficial outflow (Fig. 2a). Using this photograph, Vilímek et al. (2005) estimated a lake
117 volume between 9 and 11 million m³ at that time, whereas an unpublished estimate of the Autoridad Nacional del



118 Agua (ANA) arrived at approx. 13.1 million m³. It is assumed that the situation was essentially the same at the time of
119 the 1941 GLOF (Sect. 2.2).

120 The Cojup Valley is part of the Quilcay catchment, draining towards southwest to the city of Huaráz, capital of the
121 department of Ancash located at 3,090 m a.s.l. at the outlet to the Río Santa Valley (Callejon de Huaylas). The distance
122 between Lake Palcacocha and Huaráz is approx. 23 km, whereas the vertical drop is approx. 1,500 m. The Cojup Val-
123 ley forms a glacially shaped high-mountain valley in its upper part whilst cutting through the promontory of the Cor-
124 dillera Blanca in its lower part. 8 km downstream from Lake Palcacocha (15 km upstream of Huaráz), the landslide-
125 dammed Lake Jircacocha (4.8 million m³; Vilímek et al., 2005) existed until 1941 (Andres et al., 2018). The remnants
126 of this lake are still clearly visible in the landscape in 2017, mainly through the change in vegetation and the presence
127 of fine lake sediments (Fig. 2b). Table 1 summarizes the major characteristics of Lake Palcacocha and Lake Jircacocha
128 before the 1941 GLOF.

129 2.2 1941 multi-lake outburst flood from Lake Palcacocha

130 On 13 December 1941 part of the city of Huaráz was destroyed by a catastrophic GLOF-induced debris and mud flow,
131 with thousands of fatalities. Portocarrero (1984) gives a number of 4000 deaths, Wegner (2014) a number of 1800; but
132 this type of information has to be interpreted with care (Evans et al., 2009). The disaster was the result of a multi-lake
133 outburst flood in the upper part of the Cojup Valley. Sudden breach of the dam and the drainage of Lake Palcacocha
134 (Figs. 2c and e) led to a mass flow proceeding down the valley. Part of the eroded dam material, mostly coarse materi-
135 al, blocks and boulders, was deposited directly downstream from the moraine dam, forming an outwash fan typical for
136 moraine dam failures (Fig. 2c), whereas additional solid material forming the catastrophic mass flow was most likely
137 eroded further along the flow path (both lateral and basal erosion were observed; Wegner, 2014). The impact of the
138 flow on Lake Jircacocha led to overtopping and erosion of the landslide dam down to its base, leading to the complete
139 and permanent disappearance of this lake. The associated uptake of the additional water and debris increased the en-
140 ergy of the flow, and massive erosion occurred in the steeper downstream part of the valley, near the city of Huaráz.
141 Reports by the local communities indicate that the valley was deepened substantially, so that the traffic between vil-
142 lages was interrupted. According to Somos-Valenzuela et al. (2016), the valley bottom was lowered by as much as
143 50 m at some parts.

144 The impact area of the 1941 multi-GLOF and the condition of Lake Palcacocha after the event are well documented
145 through aerial imagery acquired in 1948 (Fig. 3). The image of Hans Kinzl acquired in 1939 (Fig. 2a) is the only record
146 of the status before the event. Additional information is available through eyewitness reports (Wegner, 2014). Howev-
147 er, as Lake Palcacocha is located in a remote, uninhabited area, no direct estimates of travel times or associated flow
148 velocities are available. Also the trigger of the sudden drainage of Lake Palcacocha remains unclear. Two mechanisms
149 appear most likely: (i) retrogressive erosion, possibly triggered by an impact wave related to calving or an ice ava-
150 lanche, resulting in overtopping of the dam (however, Vilímek et al., 2005 state that there are no indicators for such
151 an impact); or (ii) internal erosion of the dam through piping, leading to the failure.

152 2.3 Lake evolution since 1941

153 As shown on the aerial images from 1948, Lake Palcacocha was drastically reduced to a small remnant proglacial pond,
154 impounded by a basal moraine ridge within the former lake area, at a water level of 4563 m a.s.l., 47 m lower than
155 before the 1941 event (Fig. 3a). However, glacial retreat during the following decades led to an increase of the lake
156 area and volume (Vilímek et al., 2005). After reinforcement of the dam and the construction of an artificial drainage in
157 the early 1970s, a lake volume of 514,800 m³ was derived from bathymetric measurements (Ojeda, 1974). In 1974, two



158 artificial dams and a permanent drainage channel were installed, stabilizing the lake level with a freeboard of 7 m to
159 the dam crest (Portocarrero, 2014). By 2003, the volume had increased to 3.69 million m³ (Zapata et al., 2003). In the
160 same year, a landslide from the left lateral moraine caused a minor flood wave in the Cojup Valley (Fig. 2d). In 2016,
161 the lake volume had increased to 17.40 million m³ due to continued deglaciation (ANA, 2016). The potential of fur-
162 ther growth is limited since, as of 2017, Lake Palcacocha is only connected to a small regenerating glacier. Further, the
163 lake level is lowered artificially, using a set of siphons (it decreased by 3 m between December 2016 and July 2017).
164 Table 1 summarizes the major characteristics of Lake Palcacocha in 2016. The overall situation in July 2017 is illustrat-
165 ed in Fig. 2c.

166 2.4 Previous simulations of possible future GLOF process chains

167 Due to its history, recent growth, and catchment characteristics, Lake Palcacocha is considered hazardous for the
168 downstream communities, including the city of Huaráz (Fig. 2e). Whilst Vilímek et al (2005) point out that the lake
169 volume would not allow an event comparable to 1941, by 2016 the lake volume had become much larger than the
170 volume before 1941 (ANA, 2016). Even though the lower potential of dam erosion (Somos-Valenzuela et al., 2016) and
171 the non-existence of Lake Jircacocha make a 1941-magnitude event appear unlikely, the steep glacierized mountain
172 walls in the back of the lake may produce ice or rock-ice avalanches leading to impact waves, dam overtopping, ero-
173 sion, and subsequent mass flows. Investigations by Klimeš et al. (2016) of the steep lateral moraines surrounding the
174 lake indicate that failures and slides from moraines are possible at several sites, but do not have the potential to create
175 a major overtopping wave, partly due to the elongated shape of the lake. Rivas et al. (2015) elaborated on the possible
176 effects of moraine-failure induced impact waves. Recently, Somos-Valenzuela et al. (2016) have used a combination of
177 simulation approaches to assess the possible impact of process chains triggered by ice avalanching into Lake Palcac-
178 ocha on Huaráz. They considered three scenarios of ice avalanches detaching from the slope of Palcaraju (0.5, 1.0, and
179 3.0 million m³) in order to create flood intensity maps and to indicate travel times of the mass flow to various points of
180 interest. For the large scenario, the mass flow would reach the uppermost part of the city of Huaráz after approx.
181 1 h 20 min, for the other scenarios this time would increase to 2 h 50 min (medium scenario) and 8 h 40 min (small
182 scenario). Particularly for the large scenario, a high level of hazard is identified for a considerable zone near the Quil-
183 cay River, whereas zones of medium or low hazard become more abundant with the medium and small scenarios, or
184 with the assumption of a lowered lake level (Somos-Valenzuela et al., 2016). In addition, Chisolm and McKinney
185 (2018) analyzed the dynamics impulse waves generated by avalanches using FLOW-3D. A similar modelling approach
186 was applied by Frey et al. (2018) to derive a map of GLOF hazard for the Quilcay catchment. For Lake Palcacocha the
187 same ice avalanche scenarios as applied by Somos-Valenzuela et al. (2016) were employed, with correspondingly com-
188 parable results in the Cojup Valley and for the city of Huaráz.

189 3 The r.avaflow computational tool

190 r.avaflow is an open source tool for simulating the dynamics of complex mass flows in mountain areas. It employs a
191 two-phase model including solid particles and viscous fluid, making a difference to most other mass flow simulation
192 tools which build on one-phase mixture models. r.avaflow considers the interactions between the phases as well as
193 erosion and entrainment of material from the basal surface. Consequently, it is well-suited for the simulation of com-
194 plex, cascading flow-type landslide processes. The r.avaflow framework is introduced in detail by Mergili et al. (2017),
195 only those aspects relevant for the present work are explained here.

196 The Pudasaini (2012) two-phase flow model is used for propagating mass flows from at least one defined release area
197 through a Digital Terrain Model (DTM). Flow dynamics is computed through depth-averaged equations describing the



198 conservation of mass and momentum for both solid and fluid. The solid stress is computed on the basis of the Mohr-
199 Coulomb plasticity, whereas the fluid is treated with a solid-volume-fraction-gradient-enhanced non-Newtonian vis-
200 cous stress. Virtual mass due to the relative motion and acceleration, and generalized viscous drag, account for the
201 strong transfer of momentum between the phases. Also buoyancy is considered. The momentum transfer results in
202 simultaneous deformation, separation, and mixing of the phases (Mergili et al., 2018a). Pudasaini (2012) gives a full
203 description of the set of equations.

204 Certain enhancements are included, compared to the original model: for example, drag and virtual mass are computed
205 according to extended analytical functions constructed by Pudasaini (2019a, b). Additional (complementary) function-
206 alities include surface control, diffusion control, and basal entrainment (Mergili et al., 2017, 2018a, 2019). A conceptu-
207 al model is used for entrainment: thereby, the empirically derived entrainment coefficient C_E is multiplied with the
208 flow kinetic energy:

$$209 \quad q_{E,s} = C_E |T_s + T_f| \alpha_{s,E}, \quad q_{E,f} = C_E |T_s + T_f| (1 - \alpha_{s,E}). \quad (1)$$

210 $q_{E,s}$ and $q_{E,f}$ (m s^{-1}) are the solid and fluid entrainment rates, T_s and T_f (J) are the solid and fluid kinetic energies, and $\alpha_{s,E}$
211 is the solid fraction of the entrainable material (Mergili et al., 2019). Flow heights and momenta as well as the change
212 of elevation of the basal surface are updated at each time step (Mergili et al., 2017).

213 Any desired combination of solid and fluid release and entrainable heights can be defined. The main results are raster
214 maps of the evolution of solid and fluid flow heights, velocities, and entrained heights in time. Pressures and kinetic
215 energies are derived from the flow heights and velocities. Output hydrographs can be generated as an additional op-
216 tion (Mergili et al., 2018a). Spatial discretization works on the basis of GIS raster cells: the flow propagates between
217 neighbouring cells during each time step. The Total Variation Diminishing Non-Oscillatory Central Differencing
218 (TVD-NOC) Scheme (Nessyahu and Tadmor, 1990; Tai et al., 2002; Wang et al., 2004) is employed for solving the
219 model equations. This approach builds on a staggered grid, in which the system is shifted half the cell size during each
220 step in time (Mergili et al., 2018b).

221 `r.avaflow` operates as a raster module of the open source software GRASS GIS 7 (GRASS Development Team, 2019),
222 employing the programming languages Python and C as well as the R software (R Core Team, 2019). More details
223 about `r.avaflow` are provided by Mergili et al. (2017).

224 4 Simulation input

225 The simulations build on the topography, represented by a DTM, and on particular sets of initial conditions and model
226 parameters. For the DTM, we use a 5 m resolution Digital Elevation Model provided by the Peruvian Ministry of Envi-
227 ronment, MINAM (Horizons, 2013). It was deduced from recent stereo aerial photographs and airborne LiDAR. The
228 DEM is processed in order to derive a DTM representing the situation before the 1941 event. Thereby, we neglect the
229 possible error introduced by the effects of vegetation or buildings, and focus on the effects of the lakes and of erosion
230 (Fig. 4):

- 231 1. For the area of Lake Palcacocha the elevation of the lake surface is replaced by a DTM of the lake bathymetry
232 derived from ANA (2016). Possible sedimentation since that time is neglected. The photograph of Hans Kinzl
233 from 1939 (Fig. 2a) is used to reconstruct the moraine dam before the breach, and the glacier at the same time.
234 As an exact positioning of the glacier terminus is not possible purely based on the photo, the position is opti-
235 mized towards a lake volume of approx. 13 million m^3 , following the estimate of ANA. It is further assumed



- 236 that there was surficial drainage of Lake Palcacocha as suggested by Fig. 2a, i.e. the lowest part of the moraine
237 crest is set equal to the former lake level of 4,610 m a.s.l (Fig. 4b).
- 238 2. Also for Lake Jircacocha, surficial overflow is assumed (a situation that is observed for most of the recent land-
239 slide-dammed lakes in the Cordillera Blanca). On this basis the landslide dam before its breach is reconstruct-
240 ed, guided by topographic and geometric considerations. The lowest point of the dam crest is set to
241 4,130 m a.s.l. (Fig. 4c).
- 242 3. Erosional features along the flow channel are assumed to largely relate to the 1941 event. These features are
243 filled accordingly (see Table 2 for the filled volumes). In particular, the flow channel in the lower part of the
244 valley, reportedly deepened by up to 50 m in the 1941 event (Vilímek et al., 2005), was filled in order to repre-
245 sent the situation before the event in a plausible way (Fig. 4d).

246 All lakes are considered as fluid release volumes in r.avaflow. The initial level of Lake Palcacocha in 1941 is set to
247 4,610 m a.s.l., whereas the level of Lake Jircacocha is set to 4,129 m a.s.l. The frontal part of the moraine dam im-
248 pounding Lake Palcacocha and the landslide dam impounding Lake Jircacocha are considered as entrainable volumes.
249 Further, those areas filled up along the flow path (Fig. 4d) are considered entrainable, mainly following Vilímek et al.
250 (2005). However, as it is assumed that part of the material was removed through secondary processes or afterwards,
251 only 75% of the added material are allowed to be entrained. All entrained material is considered 80% solid and 20%
252 fluid per volume.

253 The reconstructed lake, breach, and entrainable volumes are shown in Tables 1 and 2. The glacier terminus in 1941
254 was located in an area where the lake depth increases by several tens of metres, so that small misestimates in the posi-
255 tion of the glacier tongue may result in large misestimates of the volume, so that some uncertainty has to be accepted.

256 We consider four scenarios:

- 257 A Retrogressive erosion, possibly induced by minor or moderate overtopping. This scenario is related to a pos-
258 sible minor impact wave, caused for example by calving of ice from the glacier front, an increased lake level
259 due to meteorological reasons, or a combination of these factors. In the simulation, the process chain is start-
260 ed by cutting an initial breach into the dam in order to initiate overtopping and erosion. The fluid phase is
261 considered as pure water.
- 262 AX Similar to Scenario A, but with the second phase considered a mixture of fine mud and water. For this pur-
263 pose, density is increased to 1,100 instead of 1,000 kg m⁻³, and a yield strength of 5 Pa is introduced (Table 3).
264 For simplicity, we still refer to this mixture as a fluid. Such changed phase characteristics may be related to
265 the input of fine sediment into the lake water (e.g. caused by a landslide from the lateral moraine as trigger-
266 ing event), but are mainly considered here in order to highlight the effects of uncertainties in the definition
267 and parameterization of the two-phase mixture flow.
- 268 B Retrogressive erosion, induced by violent overtopping. This scenario is related to a large impact wave caused
269 by a major rock/ice avalanche or ice avalanche rushing into the lake. In the simulation, the process chain is
270 initiated through a hypothetical landslide of 3 million m³ of 75% solid and 25% fluid material, following the
271 large scenario of Somos-Valenzuela et al. (2016) in terms of volume and release area. In order to be consistent
272 with Scenario A, fluid is considered as pure water.
- 273 C Internal erosion-induced failure of the moraine dam. Here, the process chain is induced by the collapse of
274 the entire reconstructed breach volume (Fig. 4b). In the simulation, this is done by considering this part of
275 the moraine not as entrainable volume, but as release volume (80% solid, 20% fluid, whereby fluid is again
276 considered as pure water).



277 Failure of the dam of Lake Jircacocha is assumed having occurred through overtopping and retrogressive erosion, in-
278 duced by the increased lake level and a minor impact wave from the flood upstream. No further assumptions of the
279 initial conditions are required in this case.

280 The model parameter values are selected in accordance with experiences gained from previous simulations with
281 *r.avaflow* for other study areas, and are summarized in Table 3. Three parameters mainly characterizing the flow fric-
282 tion (basal friction of solid δ , ambient drag coefficient C_{AD} , and fluid friction coefficient C_{FF}) and the entrainment coef-
283 ficient C_E are optimized in a spatially differentiated way to maximize the empirical adequacy of the simulations in
284 terms of estimates of impact areas, erosion depths, and flow and breach volumes. As no travel times or velocities are
285 documented for the 1941 event, we use the values given by Somos-Valenzuela et al. (2016) as a rough reference. Vary-
286 ing those four parameters while keeping the others constant helps us to capture variability while minimizing the de-
287 grees of freedom, remaining aware of possible equifinality issues (Beven, 1996; Beven and Freer, 2001).

288 A particularly uncertain parameter is the empirical entrainment coefficient C_E (Eq. 1). In order to optimize C_E , we
289 consider (i) successful prediction of the reconstructed breach volumes; and (ii) correspondence of peak discharge with
290 published empirical equations on the relation between peak discharge, and lake volume and dam height (Walder and
291 O'Connor, 1997). Table 4 summarizes these equations for moraine dams (applied to Lake Palcacocha) and landslide
292 dams (applied to Lake Jircacocha), and the values obtained for the regression and the envelope, using the volumes of
293 both lakes. We note that Table 4 reveals very large differences – roughly one order of magnitude – between regression
294 and envelope. In case of the breach of the moraine dam of Lake Palcacocha, we consider an extreme event due to the
295 steep, poorly consolidated, and maybe soaked moraine, with a peak discharge close to the envelope (approx..
296 $15,000 \text{ m}^3 \text{ s}^{-1}$). For Lake Jircacocha, in contrast, the envelope values of peak discharge do not appear realistic. However,
297 due to the high rate of water inflow from above, a value well above the regression line still appears plausible, even
298 though the usefulness of the empirical laws for this type of lake drainage can be questioned. The value of C_E optimized
299 for the dam of Lake Jircacocha is also used for entrainment along the flow path.

300 All of the computational experiments are run with 10 m spatial resolution. Only flow heights ≥ 25 cm are considered
301 for visualization and evaluation. We now describe one representative simulation result for each of the considered sce-
302 narios, thereby spanning the most plausible and empirically adequate field of simulations.

303 5 *r.avaflow* simulation results

304 5.1 Scenario A – Event induced by overtopping; fluid without yield strength

305 Outflow from Lake Palcacocha starts immediately, leading to (1) lowering of the lake level and (2) retrogressive ero-
306 sion of the moraine dam. The bell-shaped fluid discharge curve at the hydrograph profile O1 (Fig. 4) reaches its peak
307 of $18,700 \text{ m}^3 \text{ s}^{-1}$ after approx. 780 s, and then decreases to a small residual (Fig. 5a). Channel incision happens quickly –
308 53 m of lowering of the terrain at the reference point R1 occurs in the first less than 1200 s, whereas the lowering at
309 the end of the simulation is 60 m (Fig. 6a). This number represents an underestimation, compared to the reference
310 value of 76 m (Table 2). The lake level decreases by 42 m, whereby 36.5 m of the decrease occur within the first
311 1200 s. The slight underestimation, compared to the reference value of 47 m of lake level decrease, is most likely a
312 consequence of uncertainties in the topographic reconstruction. A total amount of 1.5 million m^3 is eroded from the
313 moraine dam of Lake Palcacocha, corresponding to an underestimation of 22%, compared to the reconstructed breach
314 volume. Underestimations mainly occur at both sides of the lateral parts of the eroded channel near the moraine crest
315 – an area where additional post-event erosion can be expected, so that the patterns and degree of underestimation
316 appear plausible (Fig. 7a). In contrast, some overestimation of erosion occurs in the inner part of the dam. For numeri-



317 cal reasons, some minor erosion is also simulated away from the eroded channel. The iterative optimization procedure
318 results in an entrainment coefficient $C_E = 10^{-6.75}$.

319 The deposit of much of the solid material eroded from the moraine dam directly downstream from Lake Palcacocha, as
320 observed in the field (Fig. 2c), is reasonably well reproduced by this simulation, so that the flow proceeding down-
321 valley is dominated by the fluid phase (Fig. 8). It reaches Lake Jircacocha after $t = 840$ s (Fig. 5b). As the inflow occurs
322 smoothly, there is no impact wave in the strict sense, but it is rather the steadily rising water level (see Fig. 6b for the
323 evolution of the water level at the reference point R2) inducing overtopping and erosion of the dam. This only starts
324 gradually after some lag time, at approx. $t = 1,200$ s. The discharge curve at the profile O2 (Fig. 4) reaches its pro-
325 nounced peak of $750 \text{ m}^3 \text{ s}^{-1}$ solid and $14,700 \text{ m}^3 \text{ s}^{-1}$ fluid material at $t = 2,340$ s, and then tails off slowly.

326 In the case of Lake Jircacocha, the simulated breach is clearly shifted south, compared to the observed breach. With
327 the optimized value of the entrainment coefficient $C_E = 10^{-7.15}$, the breach volume is underestimated by 24%, compared
328 to the reconstruction (Fig. 7b). Also here, this intentionally introduced discrepancy accounts for some post-event ero-
329 sion. However, we note that volumes are uncertain as the reconstruction of the dam of Lake Jircacocha – in contrast to
330 Lake Palcacocha – is a rough estimation due to lacking reference data.

331 Due to erosion of the dam of Lake Jircacocha, and also erosion of the valley bottom and slopes, the solid fraction of the
332 flow increases considerably downstream. Much of the solid material, however, is deposited in the lateral parts of the
333 flow channel, so that the flow arriving at Huaráz is fluid-dominated again (Fig. 8). The front enters the alluvial fan of
334 Huaráz at $t = 2,760$ s, whereas the broad peak of $10,500 \text{ m}^3 \text{ s}^{-1}$ of fluid and $2,000 \text{ m}^3 \text{ s}^{-1}$ of solid material (solid fraction
335 of 16%) is reached in the period between 3,600 and 3,780 s (Fig. 4; Fig. 5c). Discharge decreases steadily afterwards. A
336 total of 2.5 million m^3 of solid and 14.0 million m^3 of fluid material pass the hydrograph profile O3 until $t = 5,400$ s.
337 Referring only to the solid, this is less material than reported by Kaser and Georges (2003). However, (i) there is still
338 some material coming after, and (ii) pore volume has to be added to the solid volume, so that the order of magnitude
339 of material delivered to Huaráz corresponds to the documentation in a better way. Still, the solid ratio of the hydro-
340 graph might represent an underestimation.

341 As prescribed by the parameter optimization, the volumes entrained along the channel are in the same order of mag-
342 nitude, but lower than the reconstructed volumes summarized in Table 2: 0.7 million m^3 of material are entrained
343 upstream and 1.5 million m^3 downstream of Lake Jircacocha, and 5.3 million m^3 in the promontory. Fig. 9a summariz-
344 es the travel times and the flow velocities of the entire process chain. Frontal velocities mostly vary between 5 m s^{-1}
345 and 20 m s^{-1} , with the higher values in the steeper part below Lake Jircacocha. The low and undefined velocities di-
346 rectly downstream of Lake Jircacocha reflect the time lag of substantial overtopping. The key numbers in terms of
347 times, discharges, and volumes are summarized in Table 5.

348 5.2 Scenario AX – Event induced by overtopping; fluid with yield strength

349 Adding a yield strength of $\tau_y = 5 \text{ Pa}$ to the characteristics of the fluid substantially changes the temporal rather than
350 the spatial evolution of the process cascade. As the fluid now behaves as fine mud instead of water and is more re-
351 sistant to motion, velocities are lower, travel times are much longer, and the entrained volumes are smaller than in the
352 Scenario A (Fig. 9b; Table 5). The peak discharge at the outlet of Lake Palcacocha is reached at $t = 1,800$ s. Fluid peak
353 discharge of $8,200 \text{ m}^3 \text{ s}^{-1}$ is less than half the value yielded in Scenario A (Fig. 5d). The volume of material eroded from
354 the dam is only slightly smaller than in Scenario A (1.4 versus 1.5 million m^3). The numerically induced false positives
355 with regard to erosion observed in Scenario A are not observed in Scenario AX, as the resistance to oscillations in the
356 lake is lower with the added yield strength (Fig. 7c). Still, the major patterns of erosion and entrainment are the same.
357 Interestingly, erosion is deeper in Scenario AX, reaching 76 m at the end of the simulation (Fig. 6c) and therefore the



358 base of the entrainable material (Table 2). This is most likely a consequence of the spatially more concentrated flow
359 and therefore higher erosion rates along the centre of the breach channel, with less lateral spreading than in Scenar-
360 io A.

361 Consequently, also Lake Jircacocha is reached later than in Scenario A (Fig. 6d), and the peak discharge at its outlet is
362 delayed ($t = 4,320$ s) and lower ($7,600 \text{ m}^3 \text{ s}^{-1}$ of fluid and $320 \text{ m}^3 \text{ s}^{-1}$ of solid material) (Fig. 5e). 2.0 million m^3 of materi-
363 al are entrained from the dam of Lake Jircacocha, with similar spatial patterns as in Scenario A (Fig. 7d). Huaráz is
364 reached after $t = 4,200$ s, and the peak discharge of $5,000 \text{ m}^3 \text{ s}^{-1}$ of fluid and $640 \text{ m}^3 \text{ s}^{-1}$ of solid material at O3 occurs
365 after $t = 6,480$ s (Fig. 5f). This corresponds to a solid ratio of 11%. Interpretation of the solid ratio requires care here as
366 the fluid is defined as fine mud, so that the water content is much lower than the remaining 89%. The volumes en-
367 trained along the flow channel are similar in magnitude to those obtained in the simulation of Scenario A (Table 5).

368 5.3 Scenario B – Event induced by impact wave

369 Scenario B is based on the assumption of an impact wave from a 3 million m^3 landslide. However, due to the relatively
370 gently-sloped glacier tongue heading into Lake Palcacocha at the time of the 1941 event (Figs. 2a and 4b), only a small
371 fraction of the initial landslide volume reaches the lake, and impact velocities and energies are reduced, compared to a
372 direct impact from the steep slope. Approx. 1 million m^3 of the landslide have entered the lake until $t = 120$ s, an
373 amount which only slightly increases thereafter. Most of the landslide deposits on the glacier surface. Caused by the
374 impact wave, discharge at the outlet of Lake Palcacocha (O1) sets on at $t = 95$ s and, due to overtopping of the impact
375 wave, immediately reaches a relatively moderate first peak of $7,000 \text{ m}^3 \text{ s}^{-1}$ of fluid discharge. The main peak of
376 $16,900 \text{ m}^3 \text{ s}^{-1}$ of fluid and $2,000 \text{ m}^3 \text{ s}^{-1}$ of solid discharge occurs at $t = 1,200$ s due do the erosion of the breach channel.
377 Afterwards, discharge decreases relatively quickly to a low base level (Fig. 10a). The optimized value of $C_E = 10^{-6.75}$ is
378 used also for this scenario. The depth of erosion along the main path of the breach channel is clearly less than in the
379 Scenario A (Fig. 6e). However, Table 5 shows a higher volume of eroded dam material than the other scenarios. These
380 two contradicting patterns are explained by Fig. 11a: the overtopping due to the impact wave does not only initiate
381 erosion of the main breach, but also of a secondary breach farther north. Consequently, discharge is split among the
382 two breaches and therefore less concentrated, explaining the lower erosion at the main channel despite a larger total
383 amount of eroded material. The secondary drainage channel can also be deduced from observations (Fig. 3a), but has
384 probably played a less important role than suggested by this simulation.

385 The downstream results of Scenario B largely correspond to the results of the Scenario A, with some delay partly relat-
386 ed to the time from the initial landslide to the overtopping of the impact wave. Discharge at the outlet of Lake Jircaco-
387 cha peaks at $t = 2,700$ s (Fig. 10b), and the alluvial fan of Huaráz is reached after 3,060 s (Fig. 10c). The peak discharges
388 at O2 and O3 are similar to those obtained in the Scenario A. The erosion patterns at the dam of Lake Jircacocha
389 (again, $C_E = 10^{-7.15}$) very much resemble those yielded with the scenarios A and AX (Fig. 11b), and so does the volume
390 of entrained dam material (2.2 million m^3). The same is true for the 2.5 million m^3 of solid and 13.9 million m^3 of fluid
391 material entering the area of Huaráz until $t = 5,400$ s, according to this simulation.

392 Also in this scenario, the volumes entrained along the flow channel are very similar to those obtained in the simula-
393 tion of Scenario A. The travel times and frontal velocities – resembling the patterns obtained in Scenario A, with the
394 exception of the delay – are shown in Fig. 12a, whereas Table 5 summarizes the key numbers in terms of times, vol-
395 umes, and discharges.



396 5.4 Scenario C – Event induced by dam collapse

397 In Scenario C, we assume that the breached part of the moraine dam collapses, the collapsed mass mixes with the wa-
398 ter from the suddenly draining lake, and flows downstream. The more sudden and powerful release, compared to the
399 two other scenarios, leads to higher frontal velocities and shorter travel times (Fig. 12b; Table 5).

400 In contrast to the other scenarios, impact downstream starts earlier, as more material is released at once, instead of
401 steadily increasing retrogressive erosion and lowering of the lake level. The fluid discharge at O1 peaks at almost
402 $40,000 \text{ m}^3 \text{ s}^{-1}$ (Fig. 10d) rapidly after release. Consequently, Lake Jircacocha is reached already after 720 s, and the im-
403 pact wave in the lake evolves more quickly than in all the other scenarios considered (Fig. 6f). The lake drains with a
404 peak discharge of $15,400 \text{ m}^3 \text{ s}^{-1}$ of fluid and $830 \text{ m}^3 \text{ s}^{-1}$ of solid material after 1,680–1,740 s (Fig. 10e). In contrast to the
405 more rapid evolution of the process chain, discharge magnitudes are largely comparable to those obtained with the
406 other scenarios. The same is true for the hydrograph profile O3: the flow reaches the alluvial fan of Huaráz after
407 $t = 2,160 \text{ s}$, with a peak discharge slightly exceeding $10,000 \text{ m}^3 \text{ s}^{-1}$ of fluid and $2,000 \text{ m}^3 \text{ s}^{-1}$ of solid material between
408 $t = 2,940 \text{ s}$ and $3,240 \text{ s}$. 2.7 million m^3 of solid and 14.6 million m^3 of fluid material enter the area of Huaráz until
409 $t = 5,400 \text{ s}$, which is slightly more than in the other scenarios, indicating the more powerful dynamics of the flow (Ta-
410 ble 5). The fraction of solid material arriving at Huaráz remains low, with 16% solid at peak discharge and 15% in to-
411 tal. Again, the volumes entrained along the flow channel are very similar to those obtained with the simulations of the
412 other scenarios (Table 5).

413 6 Discussion

414 6.1 Possible trigger of the GLOF process chain

415 There is disagreement upon the trigger of the 1941 multi-lake outburst flood in the Quilcay catchment. Whereas, ac-
416 cording to contemporary reports, there is no evidence of a landslide (for example, ice avalanche) impact onto the lake
417 (Vilímek et al., 2005; Wegner, 2014), and dam rupture would have been triggered by internal erosion, some authors
418 postulate an at least small impact starting the process chain (Portocarrero, 2014; Somos-Valenzuela et al., 2016).

419 Each of the three assumed initiation mechanisms of the 1941 event, represented by the Scenarios A/AX, B, and C,
420 yields results which are plausible in principle. We consider a combination of all three mechanisms a likely cause of
421 this extreme process chain. Overtopping of the moraine dam, possibly related to a minor impact wave, leads to the
422 best correspondence of the model results with the observation, documentation, and reconstruction. Particularly the
423 signs of minor erosion of the moraine dam north of the main breach (Fig. 3a) support this conclusion: a major impact
424 wave, resulting in violent overtopping of the entire frontal part of the moraine dam, would supposedly also have led to
425 more pronounced erosion in that area, as to some extent predicted by the Scenario B. There is also no evidence for
426 strong landslide-glacier interactions (massive entrainment of ice or even detachment of the glacier tongue) which
427 would be likely scenarios in the case of a very large landslide. Anyway, the observations do not allow for substantial
428 conclusions on the volume of a hypothetical triggering landslide: as suggested by Scenario B, even a large landslide from
429 the slopes of Palcaraju or Pucaranra could have been partly alleviated on the rather gently sloped glacier tongue be-
430 tween the likely release area and Lake Palcacocha.

431 The minor erosional feature north of the main breach was already visible in the photo of Kinzl (Fig. 2a), possibly indi-
432 cating an earlier, small GLOF. It remains unclear whether it was reactivated in 1941. Such a reactivation could only be
433 directly explained by an impact wave, but not by retrogressive erosion only (A/AX) or internal failure of the dam (C) –
434 so, more research is needed here. The source area of a possible impacting landslide could have been the slopes of Pal-



435 caraju or Pucaranra (Fig. 1), or the calving glacier front (Fig. 2a). Attempts to quantify the most likely release volume
436 and material composition would be considered speculative due to the remaining difficulties in adequately simulating
437 landslide-(glacier)-lake interactions (Westoby et al., 2014). Further research is necessary in this direction. In any case,
438 a poor stability condition of the dam (factor of safety ~ 1) could have facilitated the major retrogressive erosion of the
439 main breach. A better understanding of the hydro-mechanical load applied by a possible overtopping wave and the
440 mechanical strength of the moraine dam could help to resolve this issue.

441 The downstream patterns of the flow are largely similar for each of the scenarios A, AX, B, and C, with the exception
442 of travel times and velocities. Interaction with Lake Jircacocha disguises much of the signal of process initiation. Lag
443 times between the impact of the flow front on Lake Jircacocha and the onset of substantial overtopping and erosion
444 are approx. 10 minutes in the scenarios A and B, and less than 3 minutes in the Scenario C. This clearly reflects the
445 slow and steady onset of those flows generated through retrogressive erosion. The moderate initial overtopping in
446 Scenario B seems to alleviate before reaching Lake Jircacocha. Sudden mechanical failure of the dam (Scenario C), in
447 contrast, leads to a more sudden evolution of the flow, with more immediate downstream consequences.

448 6.2 Parameter uncertainties

449 We have tried to back-calculate the 1941 event in a way reasonably corresponding to the observation, documentation
450 and reconstruction, and building on physically plausible parameter sets. Earlier work on the Huascarán landslides of
451 1962 and 1970 has demonstrated that empirically adequate back-calculations are not necessarily plausible with regard
452 to parameterization (Mergili et al., 2018b). This issue may be connected to equifinality issues (Beven, 1996; Beven and
453 Freer, 2001), and in the case of the very extreme and complex Huascarán 1970 event, by the inability of the flow mod-
454 el and its numerical solution to adequately reproduce some of the process components (Mergili et al., 2018b). In the
455 present work, however, reasonable levels of empirical adequacy and physical plausibility are achieved. Open questions
456 remain with regard to the spatial differentiation of the basal friction angle required to obtain adequate results (Ta-
457 ble 3): lower values of δ downstream from the dam of Lake Jircacocha are necessary to ensure that a certain fraction of
458 solid passes the hydrograph profile O3 and reaches Huaráz. Still, solid fractions at O3 appear rather low in all simula-
459 tions. A better understanding of the interplay between friction, drag, virtual mass, entrainment, deposition, and phase
460 separation could help to resolve this issue (Pudasaini and Fischer, 2016a, b; Pudasaini, 2019a, b).

461 The empirically adequate reproduction of the documented spatial patterns is only one part of the story (Mergili et al.,
462 2018a). The dynamic flow characteristics (velocities, travel times, hydrographs) are commonly much less well docu-
463 mented, particularly for events in remote areas which happened a long time ago. Therefore, direct references for eval-
464 uating the empirical adequacy of the dimension of time in the simulation results are lacking. However, travel times
465 play a crucial role related to the planning and design of (early) warning systems and risk reduction measures (Hof-
466 flinger et al., 2019). Comparison of the results of the scenarios A and AX (Fig. 9) reveals almost doubling travel times
467 when adding a yield stress to the fluid fraction. In both scenarios, the travel times to Huaráz are within the same order
468 of magnitude as the travel times simulated by Somos-Valenzuela et al. (2016) and therefore considered plausible, so
469 that it is hard to decide about the more adequate assumption. Even though the strategy of using the results of earlier
470 simulations as reference may increase the robustness of model results, it might also reproduce errors and inaccuracies
471 of earlier simulation attempts, and thereby confirm wrong results.

472 The large amount of more or less pure lake water would point towards the Scenario A, whereas intense mixing and
473 entrainment of fine material would favour the Scenario AX. More work is necessary in this direction, also considering
474 possible phase transformations (Pudasaini and Krautblatter, 2014). At the same time, the optimization and evaluation



475 of the simulated discharges remains a challenge. Here we rely on empirical relationships gained from the analysis of
476 comparable events (Walder and O'Connor, 1997).

477 **6.3 Implications for predictive simulations**

478 Considering what was said above, the findings from the back-calculation of the 1941 event can help us to better un-
479 derstand and constrain possible mechanisms of this extreme process chain. However, they should only be applied for
480 forward simulations in the same area or other areas with utmost care. The initial conditions and model parameters are
481 not necessarily valid for events of different characteristics and magnitudes (Mergili et al., 2018b). In the case of Lake
482 Palcacocha, the situation has changed substantially since 1941: the lake level is much lower and the volume larger,
483 and the lake is directly connected to the steep glacierized slopes, so that the impact of a hypothetical landslide could be
484 very different now. Also, the current lake is dammed by another moraine than the pre-1941 lake, with a very different
485 dam geometry (Somos-Valenzuela et al., 2016). In general, the mechanisms of the landslide impact into the lake,
486 which were not the focus of the present study, would require more detailed investigations. Ideally, such work would
487 be based on a three-phase model (Pudasaini and Mergili, 2019; considering ice as a separate phase), and consider
488 knowledge and experience gained from comparable, well-documented events. A possible candidate for such an event
489 would be the 2010 event at Laguna 513, which was back-calculated by Schneider et al. (2014). Another remaining
490 issue is the lateral spreading of the flow on the fan of Huaráz, which is overestimated in all four simulations (Figs. 8, 9,
491 and 12): the most likely reason for this is the insufficient representation of fine-scale structures such as buildings or
492 walls in the DEM, which would serve as obstacles confining the flow in lateral direction.

493 **7 Conclusions**

494 We have performed back-calculations of the documented 1941 GLOF process chain involving Lake Palcacocha and
495 Lake Jircacocha in the Quilcay catchment in the Cordillera Blanca, Perú. The key messages of this work are summa-
496 rized as follows:

- 497 • Retrogressive erosion, possibly caused by a minor impact wave, appears to be the most likely release mecha-
498 nism of the process chain, facilitated by a geotechnically poorly stable dam with a low width-to-height ratio.
499 This type of failure – a combination of the idealized scenarios considered in this work – can be inferred from
500 observations, and appears most plausible with regard to the simulation results. The identification of the trig-
501 gering process remains difficult, also because the subsequent interaction with Lake Jircacocha disguises part of
502 the respective signature downstream.
- 503 • The correspondence between simulation results and observations is reasonable, and the model parameter val-
504 ues used are physically plausible. However, considerable uncertainties remain with regard to peaks and shapes
505 of the discharge hydrographs, and to the quantification of flow velocities and travel times. Adding a yield
506 strength to the fluid phase (Scenario AX) completely changes the temporal, but not the spatial evolution of the
507 flow. Still, travel times remain in the same order of magnitude as those derived by Somos-Valenzuela et al.
508 (2016) for possible future events.
- 509 • Transfer of the findings to forward simulations in the same area or elsewhere remains a challenge due to dif-
510 ferences in the initial conditions, uncertainties of the reference data, equifinality issues, and the effects of pro-
511 cess magnitude (Mergili et al., 2018b).



512 **Code availability**

513 The model codes of r.avaflow, a manual, training data, and the necessary start scripts can be obtained from Mergili
514 (2019).

515 **Data availability**

516 The original DEM was provided by MINAM and may not be freely distributed, but all data derived within the present
517 work can be obtained by directly contacting the first author (martin.mergili@boku.ac.at).

518 **Author contribution**

519 MM developed the main ideas, defined the scenarios, did most of the data processing, simulations, and analyses, wrote
520 the major portion of the text, and prepared all the figures and tables. SP provided important ideas with regard to the
521 numerical simulations and contributed to the internal revision and optimization of the manuscript. AE contributed
522 with important ideas, conducted field work, acquired data, contributed to the writing of the introductory chapters,
523 and took part in the internal revision and optimization of the manuscript. JTF provided important contributions to the
524 internal revision and optimization of the work. AC provided important data and contributed to the internal revision
525 and optimization of the manuscript. HF contributed with important ideas and field work, data acquisition, and text
526 blocks for the introductory chapters, and took part in the internal revision and optimization of the manuscript.

527 **Competing interests**

528 The authors declare that they have no conflict of interest.

529 **Acknowledgements**

530 Part of this work was conducted within the international cooperation project “A GIS simulation model for avalanche
531 and debris flows (avaflow)” supported by the German Research Foundation (DFG, project number PU 386/3-1) and
532 the Austrian Science Fund (FWF, project number I 1600-N30). Shiva P. Pudasaini further acknowledges financial sup-
533 port from DFG through the research project “A novel and unified solution to multi-phase mass flows: U_MultiSol”.
534 The work also follows the AKTION Austria – Czech Republic project “Currently forming glacial lakes: potentially
535 hazardous entities in deglaciating high mountains” of Adam Emmer and Martin Mergili. Further, the support provided
536 by the Swiss Agency for Development and Cooperation (SDC) through Proyecto Glaciares+, is acknowledged. Adam
537 Emmer was also supported by the Ministry of Education, Youth and Sports of the Czech Republic within the National
538 Sustainability Programme I (NPU I), grant number LO1415, and the postdoc grant of the Czech Academy of Sciences.
539 Finally, we are grateful to Matthias Benedikt for comprehensive technical support in relation to r.avaflow.

540 **References**

541 ANA: Inventario Nacional de Glaciares y Lagunas – Lagunas, Ministerio de Agricultura y Riesgo, Autoridad Nacional
542 del Agua, Unidad de Glaciología y Recursos Hídricos, Huaráz, Peru, 2014.

543 ANA: Plano batimétrico de la Laguna Palcacocha. Perfil longitudinal y transversal, Ministerio de Agricultura y Riesgo,
544 Autoridad Nacional del Agua, Unidad de Glaciología y Recursos Hídricos, Huaráz, Peru, 2016.



- 545 Andres, C. N., Eyles, C. H., Jara, H., and Narro-Pérez, R.: Sedimentological analysis of Paleolake Jircacocha, Cojup
546 Valley, Cordillera Blanca, Peru. *Revista de Glaciares y Ecosistemas de Montaña*, 5, 9–26, 2018.
- 547 Beven, K.: Equifinality and Uncertainty in Geomorphological Modelling, in: *The Scientific Nature of Geomorphology:*
548 *Proceedings of the 27th Binghamton Symposium in Geomorphology, 27–29 September 1996*, John Wiley & Sons, 289–
549 313, 1996.
- 550 Beven, K., and Freer, J.: Equifinality, data assimilation, and uncertainty estimation in mechanistic modelling of com-
551 plex environmental systems using the GLUE methodology, *J. Hydrol.*, 249(1), 11–29, [https://doi.org/10.1016/S0022-](https://doi.org/10.1016/S0022-1694(01)00421-8)
552 1694(01)00421-8, 2001.
- 553 Bolch, T., Peters, J., Yegorov, A., Prafhan, B., Buchroithner, M., and Blagoveshchensky, V.: Identification of potential-
554 ly dangerous glacial lakes in the northern Tien Shan, *Nat. Hazards*, 59, 1691–1714, [https://doi.org/10.1007/s11069-011-](https://doi.org/10.1007/s11069-011-9860-2)
555 9860-2, 2011.
- 556 Breien, H., De Blasio, F. V., Elverhoi, A., and Hoeg, K.: Erosion and morphology of a debris flow caused by a glacial
557 lake outburst flood, Western Norway, *Landslides*, 5(3), 271–280, <https://doi.org/10.1007/s10346-008-0118-3>, 2008.
- 558 Broggi, J. A.: Informe preliminar sobre la exploracion y estudio de las condiciones de estabilidad de las lagunas de la
559 Cordillera Blanca, ELECTROPERU S.A., Lima, Peru, 1942.
- 560 Carey, M.: Living and dying with glaciers: people's historical vulnerability to avalanches and outburst floods in Peru.
561 *Glob. Planet. Change*, 47, 122–134, <https://doi.org/10.1016/j.gloplacha.2004.10.007>, 2005.
- 562 Carey, M., Huggel, C., Bury, J., Portocarrero, C., and Haeberli, W.: An integrated socio-environmental framework for
563 glacier hazard management and climate change adaptation: lessons from Lake 513, Cordillera Blanca, Peru, *Clim.*
564 *Change*, 112(3), 733–767, <https://doi.org/10.1007/s10584-011-0249-8>, 2012.
- 565 Carey, M., McDowell, G., Huggel, C., Jackson, M., Portocarrero, C., Reynolds, J.M., and Vicuña, L.: Integrated ap-
566 proaches to adaptation and disaster risk reduction in dynamic socio-cryospheric systems, in: *Snow and Ice-related*
567 *Hazards, Risks and Disasters*, edited by: Haeberli, W., and Whiteman, C., 219–261, Elsevier,
568 <https://doi.org/10.1016/B978-0-12-394849-6.00008-1>, 2014.
- 569 Chisolm, R. E., and McKinney, D. C.: Dynamics of avalanche-generated impulse waves: three-dimensional hydrody-
570 namic simulations and sensitivity analysis, *Nat. Hazards Earth Syst. Sci.*, 18, 1373–1393, [https://doi.org/10.5194/nhess-](https://doi.org/10.5194/nhess-18-1373-2018)
571 18-1373-2018, 2018.
- 572 Christen, M., Kowalski, J., and Bartelt, P.: RAMMS: Numerical simulation of dense snow ava-lanches in three-
573 dimensional terrain, *Cold Reg. Sci. Technol.*, 63, 1–14, <https://doi.org/10.1016/j.coldregions.2010.04.005>, 2010.
- 574 Clague, J. J., and O'Connor, J. E.: Glacier-related outburst floods, in: *Snow and Ice-related Hazards, Risks and Disas-*
575 *ters*, edited by: Haeberli, W., and Whiteman, C., 487–519, Elsevier, [https://doi.org/10.1016/B978-0-12-394849-](https://doi.org/10.1016/B978-0-12-394849-6.00014-7)
576 6.00014-7, 2014.
- 577 Concha, J. F.: Sintesis de los trabajos efectuados por la comision de las lagunas de la Cordillera Blanca, Ministerio de
578 Fomento, Comision de Control de las Lagunas de la Cordillera Blanca (CCLCB), Lima, Peru, 1952.
- 579 Emmer, A.: Geomorphologically effective floods from moraine-dammed lakes in the Cordillera Blanca, Peru, *Quat.*
580 *Sci. Rev.*, 177, 220–234, <https://doi.org/10.1016/j.quascirev.2017.10.028>, 2017.
- 581 Emmer, A., and Vilimek, V.: Review Article: Lake and breach hazard assessment for moraine-dammed lakes: an exam-
582 ple from the Cordillera Blanca (Peru), *Nat. Hazards Earth Syst. Sci.*, 13, 1551–1565, [https://doi.org/10.5194/nhess-13-](https://doi.org/10.5194/nhess-13-1551-2013)
583 1551-2013, 2013.



- 584 Emmer, A., and Vilímek, V.: New method for assessing the susceptibility of glacial lakes to outburst floods in the Cor-
585 dillera Blanca, Peru, *Hydrol. Earth Syst. Sci.*, 18, 3461–3479, <https://doi.org/10.5194/hess-18-3461-2014>, 2014.
- 586 Emmer, A., Klimeš, J., Mergili, M., Vilímek, V., and Cochachin, A.: 882 lakes of the Cordillera Blanca: an inventory,
587 classification and assessment of susceptibility to outburst flood, *Catena*, 147, 269–279,
588 <https://doi.org/10.1016/j.catena.2016.07.032>, 2016.
- 589 Emmer, A., Merkl, S., and Mergili, M.: Spatiotemporal patterns of high-mountain lakes and related hazards in western
590 Austria, *Geomorphology*, 246, 602–616, <https://doi.org/10.1016/j.geomorph.2015.06.032>, 2015.
- 591 Emmer, A., Vilímek, V., and Zapata, M. L.: Hazard mitigation of glacial lake outburst floods in the Cordillera Blanca
592 (Peru): the effectiveness of remedial works, *J. Flood Risk Manag.*, 11, 489–501, <https://doi.org/10.1111/jfr3.12241>,
593 2018.
- 594 Emmer, A., Harrison, S., Mergili, M., Allen, S., Frey, H., and Huggel, C.: A 70 year record of lake evolution and Glacial
595 Lake Outburst Floods in the Peruvian Andes, *Proc. Natl. Acad. Sci. U. S. A.*, submitted manuscript, 2019.
- 596 Evans, S. G., Bishop, N.F., Fidel Smoll, L., Valderrama Murillo, P., Delaney, K.B., and Oliver-Smith, A.: A re-
597 examination of the mechanism and human impact of catastrophic mass flows originating on Nevado Huascarán, Cor-
598 dillera Blanca, Peru in 1962 and 1970, *Eng. Geol.*, 108, 96–118, <https://doi.org/10.1016/j.enggeo.2009.06.020>, 2009.
- 599 Frey, H., Huggel, C., Chisolm, R. E., Baer, P., McArdell, B., Cochachin, A., and Portocarrero, C.: Multi-Source Glacial
600 Lake Outburst Flood Hazard Assessment and Mapping for Huaráz, Cordillera Blanca, Peru, *Front. Earth Sci.*, 6, 210,
601 <https://doi.org/10.3389/feart.2018.00210>, 2018.
- 602 Gabl, R., Seibl, J., Gerns, B., and Aufleger, M.: 3-D numerical approach to simulate the overtopping volume caused by
603 an impulse wave comparable to avalanche impact in a reservoir, *Nat. Hazards Earth Syst. Sci.*, 15, 2617–2630,
604 <https://doi.org/10.5194/nhess-15-2617-2015>, 2015.
- 605 GAPHAZ: Assessment of glacier and permafrost hazards in Mountain Regions, in: Joint Standing Group on Glacier and
606 Permafrost Hazards in High Mountains (GAPHAZ) of the International Association of Cryospheric Sciences (IACS)
607 and the International Permafrost Association (IPA), edited by: Allen, S. K., Frey, H., and Huggel, C., Zurich, Lima,
608 available online at: http://gaphaz.org/files/Assessment_Glacier_Permafrost_Hazards_Mountain_Regions.pdf, 2017.
- 609 GRASS Development Team: Geographic Resources Analysis Support System (GRASS) Software, Open Source Geospa-
610 tial Foundation Project, <https://grass.osgeo.org>, last access: 4 February 2019.
- 611 Haeberli, W.: Frequency and characteristics of glacier floods in the Swiss Alps, *Ann. Glaciol.*, 4, 85–90,
612 <https://doi.org/10.3189/S0260305500005280>, 1983.
- 613 Harrison, S., Kargel, J. S., Huggel, C., Reynolds, J., Shugar, D. H., Betts, R. A., Emmer, A., Glasser, N., Haritashya, U.
614 K., Klimeš, J., Reinhardt, L., Schaub, Y., Wilyshire, A., Regmi, D., and Vilímek, V.: Climate change and the global pat-
615 tern of moraine-dammed glacial lake outburst floods. *Cryosphere*, 12, 1195–1209, <https://doi.org/10.5194/tc-12-1195->
616 2018, 2018.
- 617 Hewitt, K., and Liu, J.: Ice-dammed lakes and outburst floods, Karakoram Himalaya: historical perspectives on emerg-
618 ing threats, *Phys. Geogr.*, 31(6), 528–551, <https://doi.org/10.2747/0272-3646.31.6.528>, 2010.
- 619 Hewitt, K.: Natural dams and outburst floods in the Karakorum Himalaya, in: *Hydrological aspects of alpine and high-*
620 *mountain areas*, edited by: Glen, J. W., IAHS Publication, 138, 259–269, 1982.
- 621 Hofflinger, A., Somos-Valenzuela, M.A., and Vallejos-Romero, A.: Response time to flood events using a social vulner-
622 ability index (ReTSVI), *Nat. Hazards Earth Syst. Sci.*, 19, 251–267, <https://doi.org/10.5194/nhess-19-251-2019>, 2019.



- 623 Horizons: Horizons South America S.A.C.: Informe Técnico del Proyecto, Consultoría Para El Levantamiento Foto-
624 gramétrico Detallado De La Sub Cuenca Del Río Quillcay Y La Ciudad De Huaráz Para El Proyecto, Imple-
625 mentación de Medidas de Adaptación al Cambio Climático y Gestión de Riesgos en la Subcuenca Quillcay (IMACC-
626 QUILLCAY) – BID-MINAM (PE-T1168), Ministerio Del Ambiente A Travel Del Fonam – Administrador De Los Re-
627 cursos Del BID, Lima, Peru, 2013.
- 628 Hubbard, B., Heald, A., Reynolds, J. M., Quincey, D., Richardson, S.D., Luyo, M.Z., Portilla, N.S., and Hambrey, M.J.:
629 Impact of a rock avalanche on a moraine-dammed proglacial lake: Laguna Safuna Alta, Cordillera Blanca, Peru, Earth
630 Surf. Proc. Landforms, 30(10), 1251–1264, <https://doi.org/10.1002/esp.1198>, 2005.
- 631 Huggel, C., Kääb, A., Haeberli, W., and Krummenacher, B.: Regional-scale GIS-models for assessment of hazards from
632 glacier lake outbursts: evaluation and application in the Swiss Alps, Nat. Hazards Earth Syst. Sci., 3, 647–662,
633 <https://doi.org/10.5194/nhess-3-647-2003>, 2003.
- 634 Iturrizaga, L.: Glacial and glacially conditioned lake types in the Cordillera Blanca, Peru: A spatiotemporal conceptual
635 approach, Prog. Phys. Geogr., 38, 602–636, <https://doi.org/10.1177/0309133314546344>, 2014.
- 636 Iverson, R. M.: The physics of debris flows, Rev. Geophys., 35, 245–296, <https://doi.org/10.1029/97RG00426>, 1997.
- 637 Kafle, J., Pokhrel, P. R., Khattri, K. B., Kattel, P., Tuladhar, B. M., and Pudasaini, S. P.: Landslide-generated tsunami
638 and particle transport in mountain lakes and reservoirs, Ann. Glaciol., 57(71), 232–244,
639 <https://doi.org/10.3189/2016AoG71A034>, 2016.
- 640 Kafle, J., Kattel, P., Mergili, M., Fischer, J.-T., and Pudasaini, S. P.: Dynamic response of submarine obstacles to two-
641 phase landslide and tsunami impact on reservoirs. Acta Mech., 1–17, <https://doi.org/10.1007/s00707-019-02457-0>,
642 2019.
- 643 Kaser, G., and Georges, C.: A potential disaster in the Icy Andes: a regrettable blunder, technical report, University of
644 Innsbruck, Austria, 2003.
- 645 Kattel, P., Khattri, K. B., Pokhrel, P. R., Kafle, J., Tuladhar, B. M., and Pudasaini, S. P.: Simu-lating glacial lake out-
646 burst floods with a two-phase mass flow model, Ann. Glaciol., 57(71), 349–358,
647 <https://doi.org/10.3189/2016AoG71A039>, 2016.
- 648 Kinzl, H., and Schneider, E.: Cordillera Blanca (Perú), Universitäts-Verlag Wagner, Innsbruck, Austria, 1950.
- 649 Klimeš, J., Novotný, J., Novotná, I., de Urries, B. J., Vilímek, V., Emmer, A., Strozzi, T., Kusák, M., Cochachin, A.,
650 Hartvich, F., and Frey, H.: Landslides in moraines as triggers of glacial lake outburst floods: example from Palcacocha
651 Lake (Cordillera Blanca, Peru), Landslides, 13(6), 1461–1477, <https://doi.org/10.1007/s10346-016-0724-4>, 2016.
- 652 McDougall, S., and Hungr, O.: A Model for the Analysis of Rapid Landslide Motion across Three-Dimensional Terrain,
653 Can. Geotech. J., 41, 1084–1097, <https://doi.org/10.1139/t04-052>, 2004.
- 654 Mergili, M.: r.avaflow – The open source mass flow simulation model, <https://www.avaflow.org/>, last access: 9 July
655 2019.
- 656 Mergili, M., and Schneider, J. F.: Regional-scale analysis of lake outburst hazards in the southwestern Pamir, Tajiki-
657 stan, based on remote sensing and GIS, Nat. Hazards Earth Syst. Sci., 11, 1447–1462, <https://doi.org/10.5194/nhess-11-1447-2011>, 2011.
- 659 Mergili, M., Schneider, D., Worni, R., and Schneider, J.F.: Glacial Lake Outburst Floods (GLOFs): challenges in predic-
660 tion and modelling, in: Proceedings of the 5th International Conference on Debris-Flow Hazards Mitigation: Mechan-



- 661 ics, Prediction and Assessment, Padova, June 14–17, 2011, edited by: Genevois, R., Hamilton, D. L., and Prestininzi,
662 A., Italian Journal of Engineering Geology and Environment – Book, 973–982, 2011.
- 663 Mergili, M., Müller, J. P., and Schneider, J. F.: Spatio-temporal development of high-mountain lakes in the headwaters
664 of the Amu Darya river (Central Asia), *Glob. Planet. Change*, 107, 13–24,
665 <https://doi.org/10.1016/j.gloplacha.2013.04.001>, 2013.
- 666 Mergili, M., Fischer, J.-T., Krenn, J., and Pudasaini, S. P.: r.avaflow v1, an advanced open source computational
667 framework for the propagation and interaction of two-phase mass flows, *Geosci. Model Dev.*, 10, 553–569,
668 <https://doi.org/10.5194/gmd-10-553-2017>, 2017.
- 669 Mergili, M., Emmer, A., Juřicová, A., Cochachin, A., Fischer, J.-T., Huggel, C., and Pudasaini, S. P.: How well can we
670 simulate complex hydro-geomorphic process chains? The 2012 multi-lake outburst flood in the Santa Cruz Valley
671 (Cordillera Blanca, Perú), *Earth Surf. Process. Landf.*, 43(7), 1373–1389, <https://doi.org/10.1002/esp.4318>, 2018a.
- 672 Mergili, M., Frank, B., Fischer, J.-T., Huggel, C., and Pudasaini, S. P.: Computational experiments on the 1962 and
673 1970 landslide events at Huascarán (Peru) with r.avaflow: Lessons learned for predictive mass flow simulations, *Geo-*
674 *morphology*, 322, 15–28, <https://doi.org/10.1016/j.geomorph.2018.08.032>, 2018b.
- 675 Mergili, M., Jaboyedoff, M., Pullarello, J., and Pudasaini, S. P.: Back-calculation of the 2017 Piz Cengalo-Bondo land-
676 slide cascade with r.avaflow, *Nat. Hazards Earth Syst. Sci. Discuss.*, <https://doi.org/10.5194/nhess-2019-204>, in review,
677 2019.
- 678 Nesyahu, H., and Tadmor, E.: Non-oscillatory central differencing for hyperbolic conservation laws, *J. Comput.*
679 *Phys.*, 87, 408–463, [https://doi.org/10.1016/0021-9991\(90\)90260-8](https://doi.org/10.1016/0021-9991(90)90260-8), 1990.
- 680 Ojeda, N.: Consolidacion laguna Palcacocha, ELECTROPERU S.A., Unidad de glaciologia y seguridad de lagunas,
681 Huaráz, Peru, 1974.
- 682 Oppenheim, V.: Sobre las Lagunas de Huaráz, *Boletin de la Sociedad Geologica del Peru*, 19, 68–80, 1946.
- 683 Pitman, E.B., and Le, L.: A two-fluid model for avalanche and debris flows. *Philos. Trans. R. Soc. A*, 363, 1573–1601,
684 <https://doi.org/10.1098/rsta.2005.1596>, 2005.
- 685 Portocarrero, C.: Seminario desastres naturales – geologia, causas, efectos y prevenciones, ELECTROPERU S.A., Unidad
686 de glaciologia y seguridad de lagunas, Huaráz, Peru, 1984.
- 687 Portocarrero, C.: The Glacial Lake Handbook: Reducing Risk from Dangerous Glacial Lakes in the Cordillera Blanca,
688 Peru, Technical Report, United States Agency for International Development, Global Climate Change Office, Climate
689 Change Resilient Development Project, Washington D.C., 2014.
- 690 Pudasaini, S. P.: A general two-phase debris flow model, *J. Geophys. Res. Earth Surf.*, 117, F03010,
691 <https://doi.org/10.1029/2011JF002186>, 2012.
- 692 Pudasaini, S. P.: A full description of generalized drag in mixture mass flows, *Phys. Fluids*, submitted manuscript,
693 2019a.
- 694 Pudasaini, S. P.: A fully analytical model for virtual mass force in mixture flows, *Int. J. Multiph. Flow*, 113, 142–152,
695 <https://doi.org/10.1016/j.ijmultiphaseflow.2019.01.005>, 2019b.
- 696 Pudasaini, S. P., and Hutter, K.: *Avalanche Dynamics: Dynamics of rapid flows of dense granular avalanches*, Springer,
697 2007.



- 698 Pudasaini, S. P., and Krautblatter, M.: A two-phase mechanical model for rock-ice avalanches, *J. Geophys. Res. Earth*
699 *Surf.*, 119, doi:10.1002/2014JF003183, 2014.
- 700 Pudasaini, S. P., and Fischer, J.-T.: A mechanical model for phase-separation in debris flow, arXiv:1610.03649, 2016a.
- 701 Pudasaini, S.P., and Fischer, J.-T.: A mechanical erosion model for two-phase mass flows, arXiv:1610.01806, 2016b.
- 702 Pudasaini, S.P., and Mergili, M.: A Multi-Phase Mass Flow Model, *J. Geophys. Res. Earth Surf.*, submitted manuscript,
703 2019.
- 704 R Core Team: R: A Language and Environment for Statistical Computing, R Foundation for Statistical Computing,
705 Vienna, Austria, <https://www.r-project.org/>, last access: 4 February 2019.
- 706 Richardson, S. D., and Reynolds, J. M.: An overview of glacial hazards in the Himalayas, *Quat. Int.*, 65/66, 31–47,
707 [https://doi.org/10.1016/S1040-6182\(99\)00035-X](https://doi.org/10.1016/S1040-6182(99)00035-X), 2000.
- 708 Rivas, D. S., Somos-Valenzuela, M. A., Hodges, B.R., and McKinney, D. C.: Predicting outflow induced by moraine
709 failure in glacial lakes: the Lake Palcacocha case from an uncertainty perspective, *Nat. Hazards Earth Syst. Sci.*, 15,
710 1163–1179, <https://doi.org/10.5194/nhess-15-1163-2015>, 2015.
- 711 Savage, S. B., and Hutter, K.: The motion of a finite mass of granular material down a rough incline, *J. Fluid Mech.*,
712 199, 177–215, <https://doi.org/10.1017/S0022112089000340>, 1989.
- 713 Schaub, Y., Huggel, C., and Cochachin, A.: Ice-avalanche scenario elaboration and uncertainty propagation in numeri-
714 cal simulation of rock-/ice-avalanche-induced impact waves at Mount Hualcán and Lake 513, Peru, *Landslides*, 13,
715 1445–1459, <https://doi.org/10.1007/s10346-015-0658-2>, 2016.
- 716 Schneider, D., Huggel, C., Cochachin, A., Guillén, S., and García, J.: Mapping hazards from glacier lake outburst floods
717 based on modelling of process cascades at Lake 513, Carhuaz, Peru, *Adv. Geosci.*, 35, 145–155,
718 <https://doi.org/10.5194/adgeo-35-145-2014>, 2014.
- 719 Somos-Valenzuela, M. A., Chisolm, R. E., Rivas, D. S., Portocarrero, C., and McKinney, D. C.: Modeling a glacial lake
720 outburst flood process chain: the case of Lake Palcacocha and Huaráz, Peru, *Hydrol. Earth Syst. Sci.*, 20, 2519–2543,
721 <https://doi.org/10.5194/hess-20-2519-2016>, 2016.
- 722 Tai, Y. C., Noelle, S., Gray, J. M. N. T., and Hutter, K.: Shock-capturing and front-tracking methods for granular ava-
723 lanches, *J. Comput. Phys.*, 175(1), 269–301, <https://doi.org/10.1006/jcph.2001.6946>, 2002.
- 724 Takahashi, T., Nakagawa, H., Harada, T., and Yamashiki, Y.: Routing debris flows with particle segregation, *J. Hy-
725 draul. Res.*, 118, 1490–1507, [https://doi.org/10.1061/\(ASCE\)0733-9429\(1992\)118:11\(1490\)](https://doi.org/10.1061/(ASCE)0733-9429(1992)118:11(1490)), 1992.
- 726 Vilímek, V., Zapata, M. L., Klimeš, J., Patzelt, Z., and Santillán, N.: Influence of glacial retreat on natural hazards of
727 the Palcacocha Lake area, Peru, *Landslides*, 2(2), 107–115, <https://doi.org/10.1007/s10346-005-0052-6>, 2005.
- 728 Voellmy, A.: Über die Zerstörungskraft von Lawinen, *Schweizerische Bauzeitung*, 73, 159–162, 212–217, 246–249,
729 280–285, 1955.
- 730 Walder, J. S., and O'Connor, J. E.: Methods for predicting peak discharge of floods caused by failure of natural and
731 constructed earthen dams, *Water Resour. Res.*, 33(10), 2337–2348, <https://doi.org/10.1029/97WR01616>, 1997.
- 732 Wegner, S. A.: Lo Que el Agua se Llevó: Consecuencias y Lecciones del Aluvión de Huaráz de 1941, Technical Note 7
733 of the series “Technical Notes on Climate Change”, Ministry of Environment, Lima, Peru, 2014.



- 734 Wang, Y., Hutter, K., and Pudasaini, S. P.: The Savage-Hutter theory: A system of partial differential equations for
735 avalanche flows of snow, debris, and mud, *ZAMM – J. Appl. Math. Mech.*, 84(8), 507–527,
736 <https://doi.org/10.1002/zamm.200310123>, 2004.
- 737 Westoby, M. J., Glasser, N. F., Brasington, J., Hambrey, M. J., Quincey, D. J., and Reynolds, J. M.: Modelling outburst
738 floods from moraine-dammed glacial lakes, *Earth-Sci. Rev.*, 134, 137–159,
739 <https://doi.org/10.1016/j.earscirev.2014.03.009>, 2014.
- 740 Worni, R., Huggel, C., Clague, J. J., Schaub, Y., and Stoffel, M.: Coupling glacial lake impact, dam breach, and flood
741 processes: A modeling perspective, *Geomorphology*, 224, 161–176, <https://doi.org/10.1016/j.geomorph.2014.06.031>,
742 2014.
- 743 Zapata, M. L.: Lagunas con obras de seguridad en la Cordillera Blanca, INGEOMIN, glaciología y seguridad de lagunas,
744 Huaráz, Peru, 1978.
- 745 Zapata, M. L., Gómez, R. J. L., Santillán, N. P., Espinoza, H. V., and Huamaní, A.H.: Evaluacion del estado de los glaci-
746 ares en la cabecera de la laguna Palcacocha, Informe tecnico, INRENA, INGEMMET, Huaráz, Peru, 2003.
- 747



748 Tables

749 Table 1. Characteristics of Lake Palcacocha (1941 and 2016) and Lake Jircacocha (1941), and changes due to the 1941
750 GLOF. Topographic reconstruction according to field observations, historic photographs, Vilímek et al. (2005), ANA
751 (2016).

| Parameter | Lake Palcacocha at 1941 GLOF | Lake Palcacocha 2016 | Lake Jircacocha at 1941 GLOF |
|--|---------------------------------|-------------------------|---------------------------------|
| Lake level elevation (m a.s.l.) | 4,610 | 4,563 | ~4,130 |
| Surface area (10 ³ m ²) | 303 | 514 | 215 |
| Lake volume (10 ⁶ m ³) | 12.9 ¹⁾ | 17.4 | 3.3 |
| GLOF volume (10 ⁶ m ³) | 10.9 ²⁾ | – | 3.3 |
| Max. lake depth (m) | 108 ³⁾ | 71 | 33 |
| Lowering of lake level (m) | 47 ²⁾ | – | 33 |

752 ¹⁾ Reference values differ among sources: according to Vilímek et al. (2005), the volume of Lake Palcacocha in 1941
753 was 9–11 million m³, whereas a reconstruction of ANA resulted in 13.1 million m³. In contrast, Vilímek et al. (2005)
754 estimate a pre-failure volume of 4.8 million m³ for Lake Jircacocha, whereas, according to ANA, the volume was only
755 3.0 million m³.

756 ²⁾ Computed from the difference between the pre-1941 lake level and the modern lake level (before mitigation) of
757 4563 m. A reconstruction of ANA in 1948 resulted in a residual lake volume of approx. 100,000 m³ and a residual
758 depth of 17 m, both much smaller than derived through the reconstruction in the present work. One of the reasons for
759 this discrepancy might be the change of the glacier in the period 1941–1948.

760 ³⁾ This value is highly uncertain and might represent an overestimation: the maximum depth of the lake strongly de-
761 pends on the exact position of the glacier terminus, which was most likely located in an area of increasing lake depth
762 in 1941.

763



764 Table 2. Reference information used for back-calculation of the 1941 process chain.

| Parameter | Value | Remarks | References |
|--|-----------------------------------|---|---------------------------------------|
| Impact area | 4.3 km ² ¹⁾ | Mapped from post-event aerial images | Servicio Aerofotogramétrico Nacional |
| Breach volume – Palcacocha | 2.0 million m ³ | Comparison of pre- and post-event DTMs | Topographic reconstruction (Sect. 4) |
| Breach depth – Palcacocha | 76 m | Elevation change at reference point R1 (Fig. 4) | Topographic reconstruction (Sect. 4) |
| Breach volume – Jircacocha | 2.8 million m ³ | Comparison of pre- and post-event DTMs | Topographic reconstruction (Sect. 4) |
| Material entrained upstream from Lake Jircacocha | 1.0 million m ³ | Maximum, value might be much lower | Topographic reconstruction (Sect. 4) |
| Material entrained downstream from Lake Jircacocha | 3.1 million m ³ | Maximum, value might be much lower | Topographic reconstruction (Sect. 4) |
| Material entrained in promontory | 7.3 million m ³ | Maximum, value might be much lower | Topographic reconstruction (Sect. 4) |
| Maximum depth of entrainment in promontory | 50 m | Rough estimate | Somos-Valenzuela et al. (2016) |
| Material arriving at Huaráz | 4–6 million m ³ | | Kaser and Georges (2003) |

765 ¹⁾ Includes the surface of Lake Palcacocha

766



767 Table 3. Key model parameters applied to the simulations in the present work. Where three values are given, the first
 768 value applies to the glacier, the second value to the remaining area upstream of the dam of Lake Jircacocha, and the
 769 third value to the area downstream of the dam of Lake Jircacocha.

| Symbol | Parameter | Unit | Value |
|-----------|--|--------------------------------|---|
| ρ_S | Solid material density (grain density) | kg m ⁻³ | 2,700 |
| ρ_F | Fluid material density | kg m ⁻³ | 1,000 ¹⁾ |
| φ | Internal friction angle | Degree | 28 |
| δ | Basal friction angle | Degree | 6, 12, 7 |
| ν | Kinematic viscosity of fluid | m ² s ⁻¹ | ~0 |
| τ_y | Yield strength of fluid | Pa | 0 ²⁾ |
| C_{AD} | Ambient drag coefficient | – | 0.02, 0.005, 0.005 |
| C_{FF} | Fluid friction coefficient | – | 0.001, 0.004, 0.004 |
| C_E | Entrainment coefficient | – | 10 ^{-6.75} ³⁾ , 10 ^{-7.15} ⁴⁾ |

770 ¹⁾ The fluid material density is set to 1,100 kg m⁻³ in Scenario AX.

771 ²⁾ The yield strength of the fluid phase is set to 5 Pa in Scenario AX.

772 ³⁾ This value applies to the dam of Lake Palcacocha.

773 ⁴⁾ This value applies to all other areas.

774



775 Table 4. Empirical relationships for the peak discharge in case of breach of moraine and landslide dams (Walder and
 776 O'Connor, 1997), and the peak discharges estimated for Lake Palcacocha and Lake Jircacocha. q_p = peak discharge
 777 ($\text{m}^3 \text{s}^{-1}$), V = total volume of water passing through the breach (m^3); D = drop of lake level (m); REG = regression;
 778 ENV = envelope. The values of V and D for the two lakes are summarized in Table 1. See also Rivas et al. (2015).

| Moraine | a_{REG} | a_{ENV} | b | q_p Palcacocha REG ($\text{m}^3 \text{s}^{-1}$) | q_p Palcacocha ENV ($\text{m}^3 \text{s}^{-1}$) |
|-------------------------------|------------------|------------------|------|---|---|
| $q^p = a \cdot V^b$ | 0.045 | 0.22 | 0.66 | 2,231 | 10,905 |
| $q^p = a \cdot D^b$ | 60.3 | 610 | 0.84 | 1,531 | 15,484 |
| $q^p = a \cdot (V \cdot D)^b$ | 0.19 | 1.1 | 0.47 | 2,560 | 14,819 |
| Landslide | a_{REG} | a_{ENV} | b | q_p Jircacocha REG ($\text{m}^3 \text{s}^{-1}$) | q_p Jircacocha ENV ($\text{m}^3 \text{s}^{-1}$) |
| $q^p = a \cdot V^b$ | 1.6 | 46 | 0.46 | 1,638 | 47,101 |
| $q^p = a \cdot D^b$ | 6.7 | 200 | 1.73 | 2,839 | 84,734 |
| $q^p = a \cdot (V \cdot D)^b$ | 0.99 | 25 | 0.4 | 1,662 | 41,973 |

779



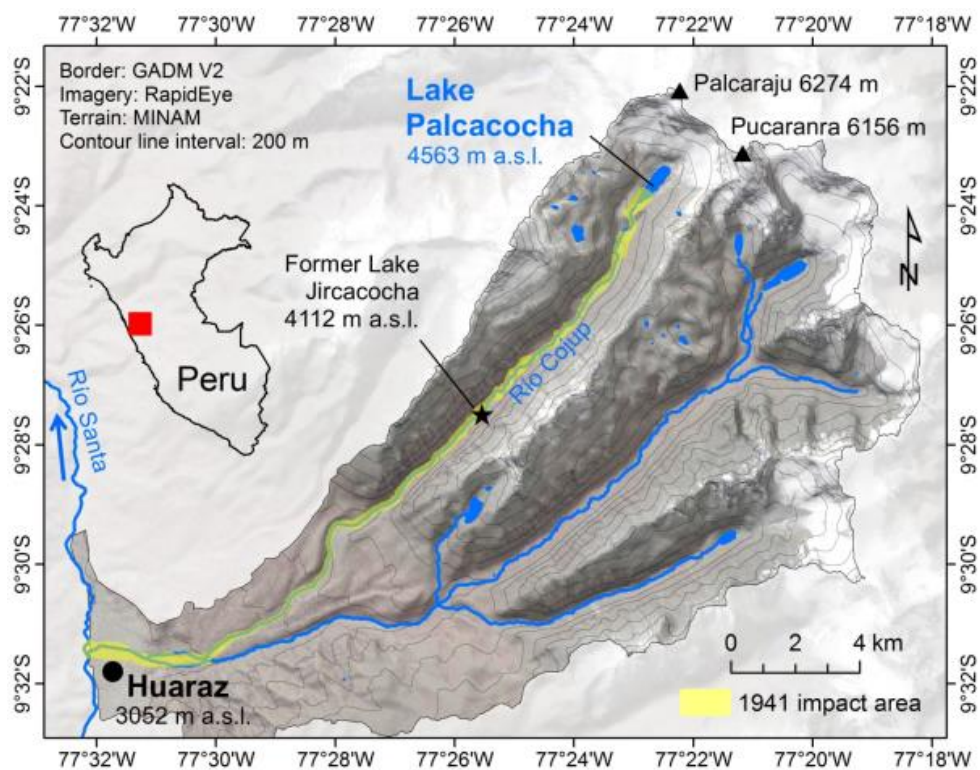
780 Table 5. Summary of the key results obtained with the computational experiments A–C. Refer to Tables 1 and 2 for the
 781 volumes involved, and to Table 4 for empirically expected peak discharges. Note that all entrained volumes are com-
 782 posed of 80% of solid and 20% of fluid material in terms of volume.

| Scenario | A | AX | B | C |
|---|---------------|---------------|----------------------|---------------|
| Description | Overtopping | Overtopping | Impact wave | Dam collapse |
| Entrained volume Lake Palcacocha dam (m ³) | 1.5 million | 1.4 million | 2.7 million | – |
| Fluid peak discharge at outlet of Lake Palcacocha (m ³ s ⁻¹) | 19,000 | 8,200 | 17,000 ¹⁾ | 38,000 |
| Entrained volume Lake Jircacocha dam (m ³) | 2.2 million | 2.0 million | 2.2 million | 2.2 million |
| Fluid peak discharge at outlet of Lake Jircacocha (m ³ s ⁻¹) | 14,700 | 7,600 | 15,000 | 15,400 |
| Material entrained up-stream from Lake Jircacocha (m ³) | 0.7 million | 0.7 million | 0.7 million | 0.7 million |
| Material entrained down-stream from Lake Jircacocha (m ³) | 1.5 million | 1.3 million | 1.5 million | 1.5 million |
| Material entrained in promontory (m ³) | 5.3 million | 5.3 million | 5.3 million | 5.3 million |
| Travel time to Huaráz (s) Start (Peak) | 2,760 (3,660) | 4,200 (6,480) | 3,060 (4,080) | 2,160 (3,060) |
| Solid delivered to Huaráz (m ³) | 2.5 million | 2.6 million | 2.5 million | 2.7 million |

783 ¹⁾ Peak of initial overtopping as response to the impact wave: 7,000 m³ s⁻¹

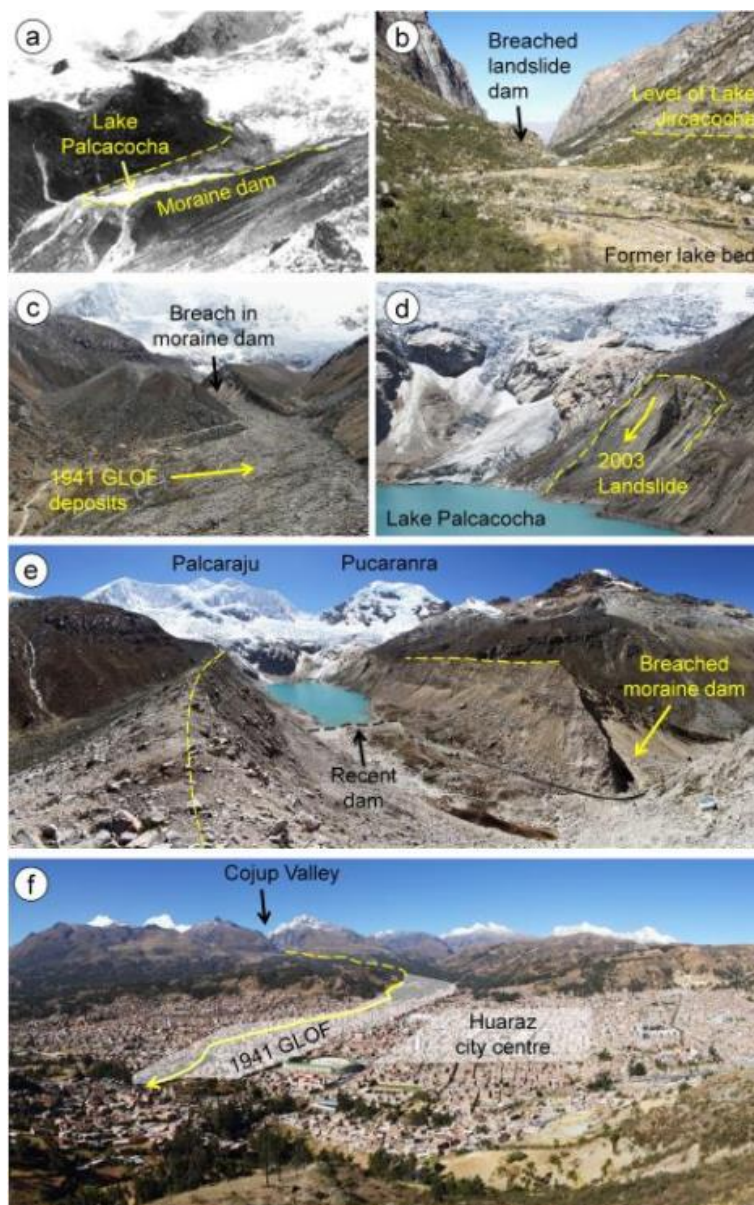


784 **Figures**



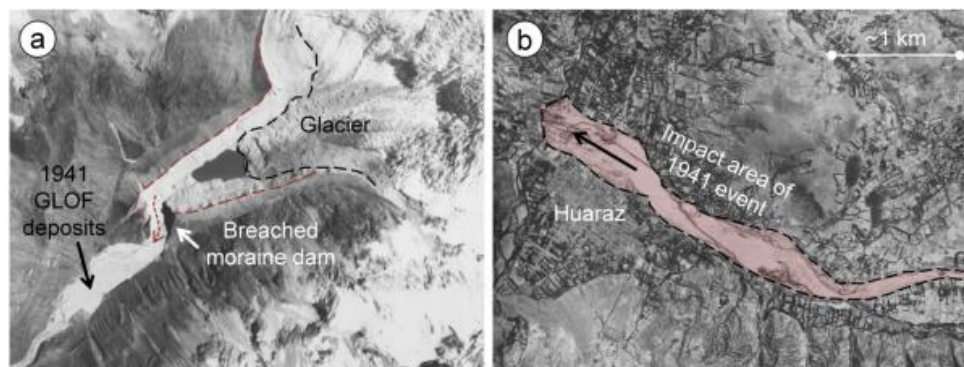
785
786 Fig. 1. Location and main geographic features of the Quilcay catchment with Lake Palcacocha and the former Lake
787 Jircacocha.

788



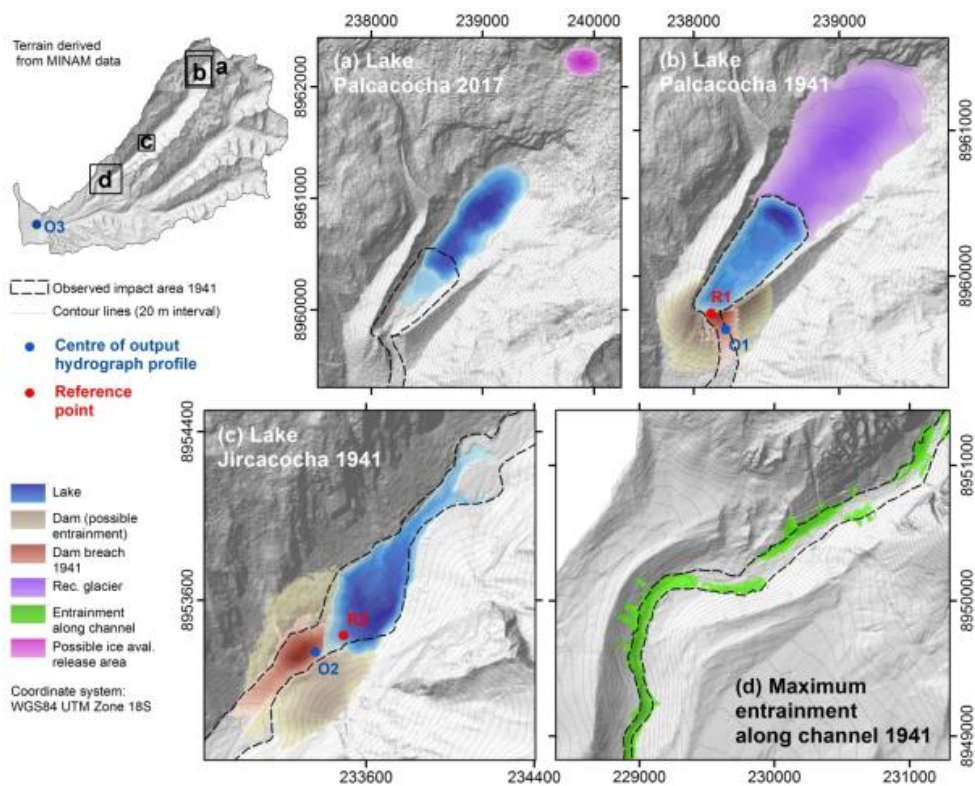
789
790
791
792
793
794
795
796
797

Fig. 2. The Quilcay catchment from Lake Palcacocha down to Huaráz. (a) Lake Palcacocha in 1939, two years prior to the 1941 event. (b) The site of former Lake Jircacocha with the breached landslide dam and the former lake level. (c) Breached moraine dam and 1941 GLOF deposits, seen from downstream. (d) Left lateral moraine of Lake Palcacocha with landslide area of 2003. (e) Panoramic view of Lake Palcacocha, with the breach in the moraine dam and the modern lake impounded by a smaller terminal moraine and two artificial dams. (f) Panoramic view of Huaráz with city centre and approximate impact area of the 1941 event. Photos: (a) Hans Kinzl, 1939 (Kinzl and Schneider, 1950); (b) Martin Mergili, July 2017; (c) Gisela Eberhard, July 2018; (d)–(f): Martin Mergili, July 2017.

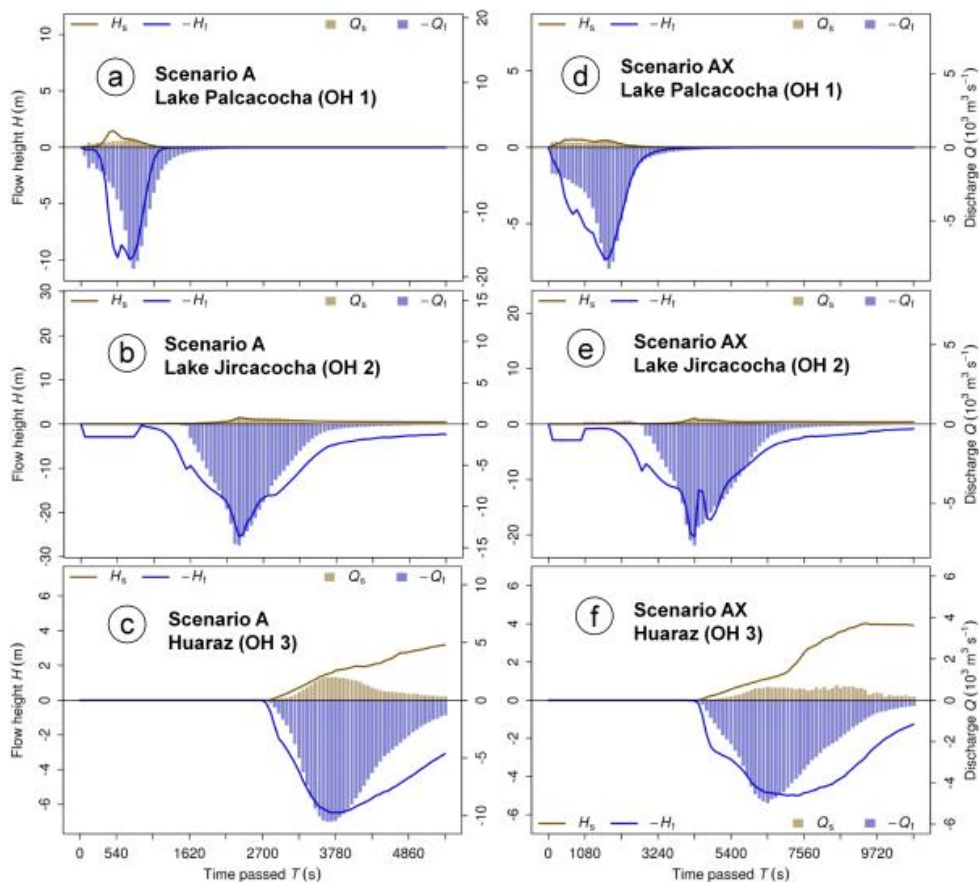


798
799 Fig. 3. Situation in 1948, seven years after the 1941 event. (a) Residual Lake Palcacocha, and traces of the 1941 event.
800 (b) Huaráz with the impact area of the 1941 event. Imagery source: Servicio Aerofotogramétrico Nacional, Perú.

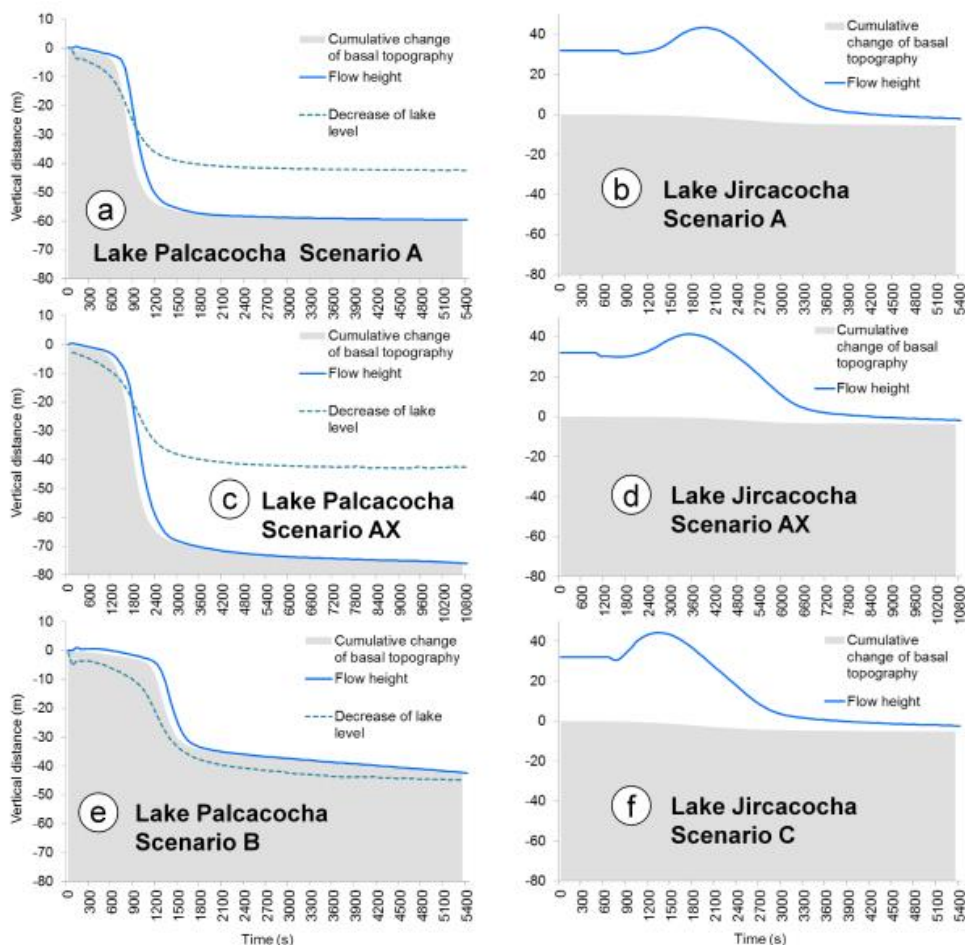
801



802
803 Fig. 4. Reconstruction of lakes and topography. (a) Lake Palcacocha in 2017. (b) Lake Palcacocha before the 1941
804 event. (c) Lake Jircacocha before the 1941 event. (d) Part of the promontory section of the Cojup Valley, with lower-
805 ing of the valley bottom by up to 50 m. The possible rock avalanche release area is shown in (a) for clarity, but is ap-
806 plied to the 1941 situation.
807



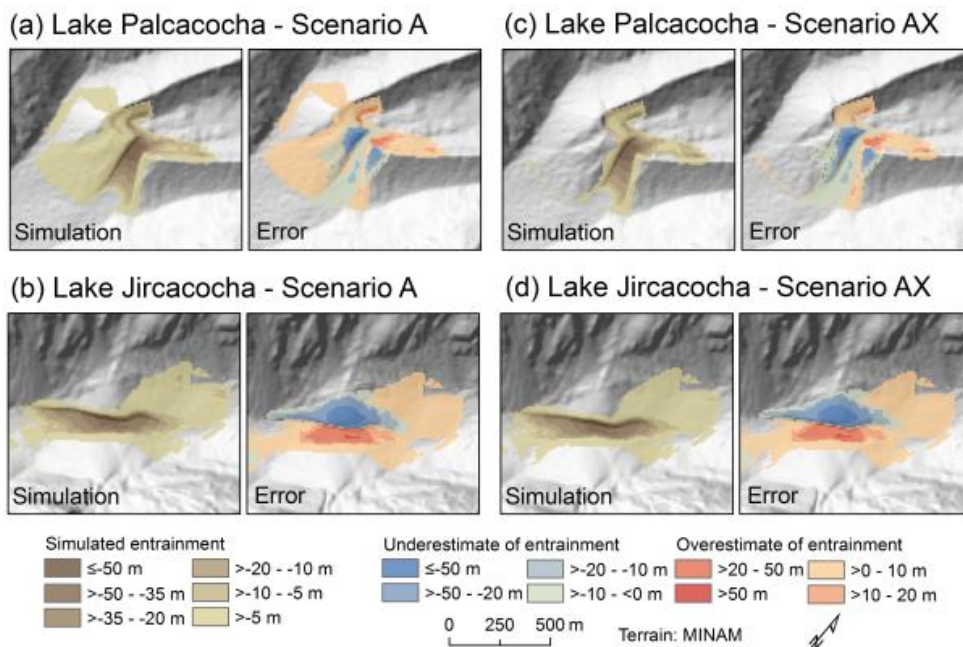
808
809 Fig. 5. Hydrographs of moraine dam failure of Lake Palcacocha (a, d), landslide dam failure of Lake Jircacocha (b, e),
810 and the flow entering the urban area of Huaráz (c, f) for the scenarios A and AX. Note that, for clarity, fluid flow
811 heights and discharges are plotted in negative direction.
812



813

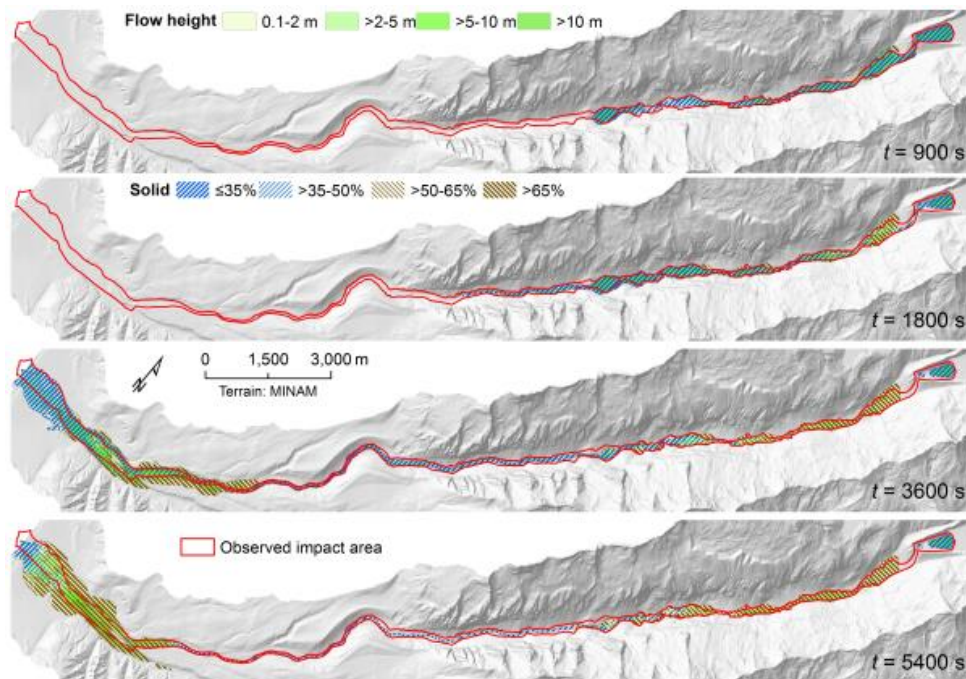
814 Fig. 6. Evolution of flow height and basal topography at the outlets of Lake Palcacocha (reference point R1 in Fig. 4b),
815 and Lake Jircacocha (reference point R2 in Fig. 4c). The reference points are placed in a way to best represent the evo-
816 lution of the breach in the dam for Lake Palcacocha, and the evolution of the impact wave for Lake Jircacocha. Addi-
817 tionally, the evolution of the lake level is shown for Lake Palcacocha. Note that the result for Scenario B is only dis-
818 played for Lake Palcacocha (e), whereas the result for Scenario C is only illustrated for Lake Jircacocha (f). The vertical
819 distance displayed on the y axis refers to the terrain height or the lake level at the start of the simulation, respectively,
820 whereby the flow height is imposed onto the topography. In Scenario B, the initial impact wave at the dam of Lake
821 Palcacocha is only poorly represented due to the low temporal resolution of the simulation, and due to blurring by
822 numerical effects (e).

823

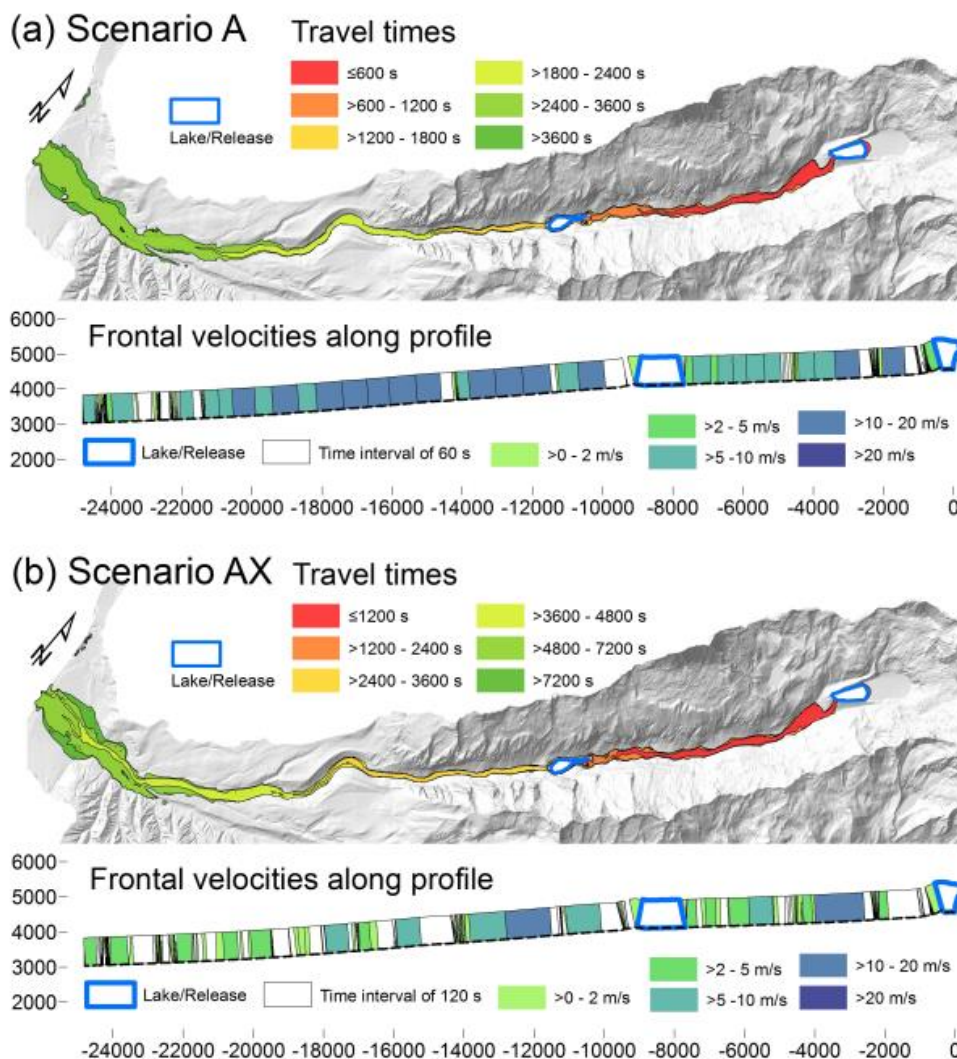


824 Fig. 7. Simulated versus reconstructed entrainment patterns for the scenarios A and AX. The total entrained height
 825 and the difference between simulated and reconstructed entrainment (error) are shown. (a) Lake Palcacocha, Scenario
 826 A. (b) Lake Jircacocha, Scenario A. (c) Lake Palcacocha, Scenario AX. (d) Lake Jircacocha, Scenario AX.
 827

828

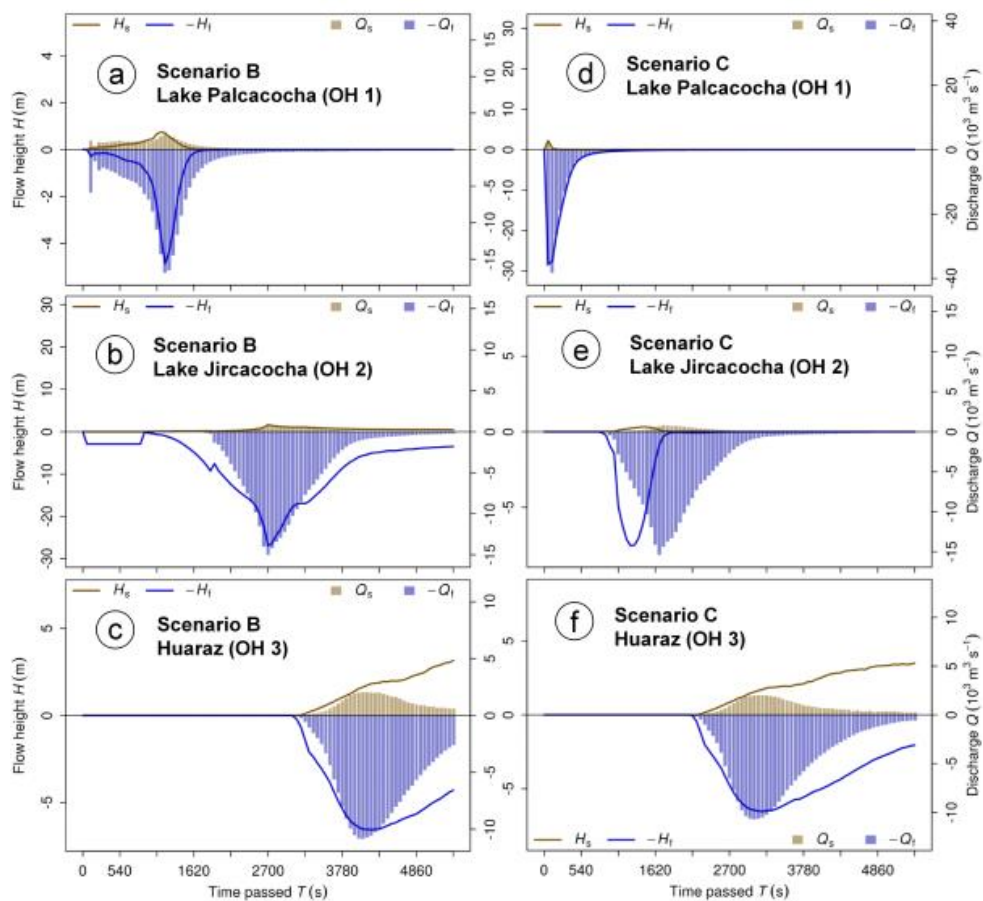


829
830 Fig. 8. Evolution of the flow in space and time (Scenario A).
831



832
 833
 834
 835

Fig. 9. Travel times and frontal velocities for the scenarios (a) A and (b) AX. Void fields in the profile graph refer to areas without clearly defined flow front.

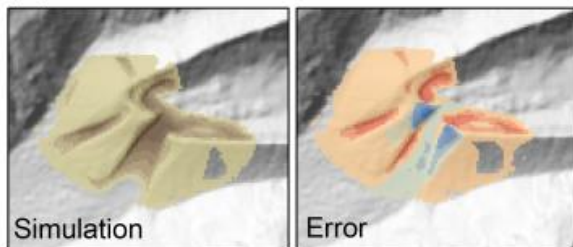


836
837 Fig. 10. Hydrographs of moraine dam failure of Lake Palcacocha (a, d), landslide dam failure of Lake Jircacocha (b, e),
838 and the flow entering the urban area of Huaráz (c, f) for the scenarios B and C. Note that, for clarity, fluid flow heights
839 and discharges are plotted in negative direction.

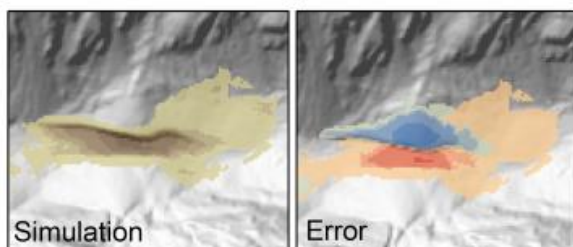
840



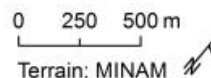
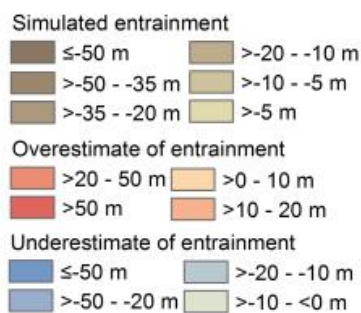
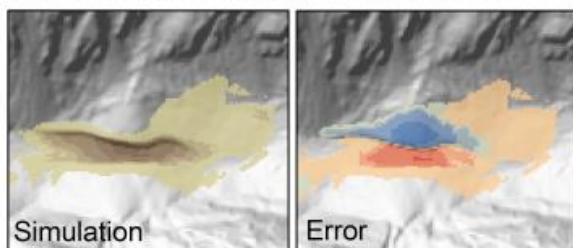
(a) Lake Palcacocha - Scenario B



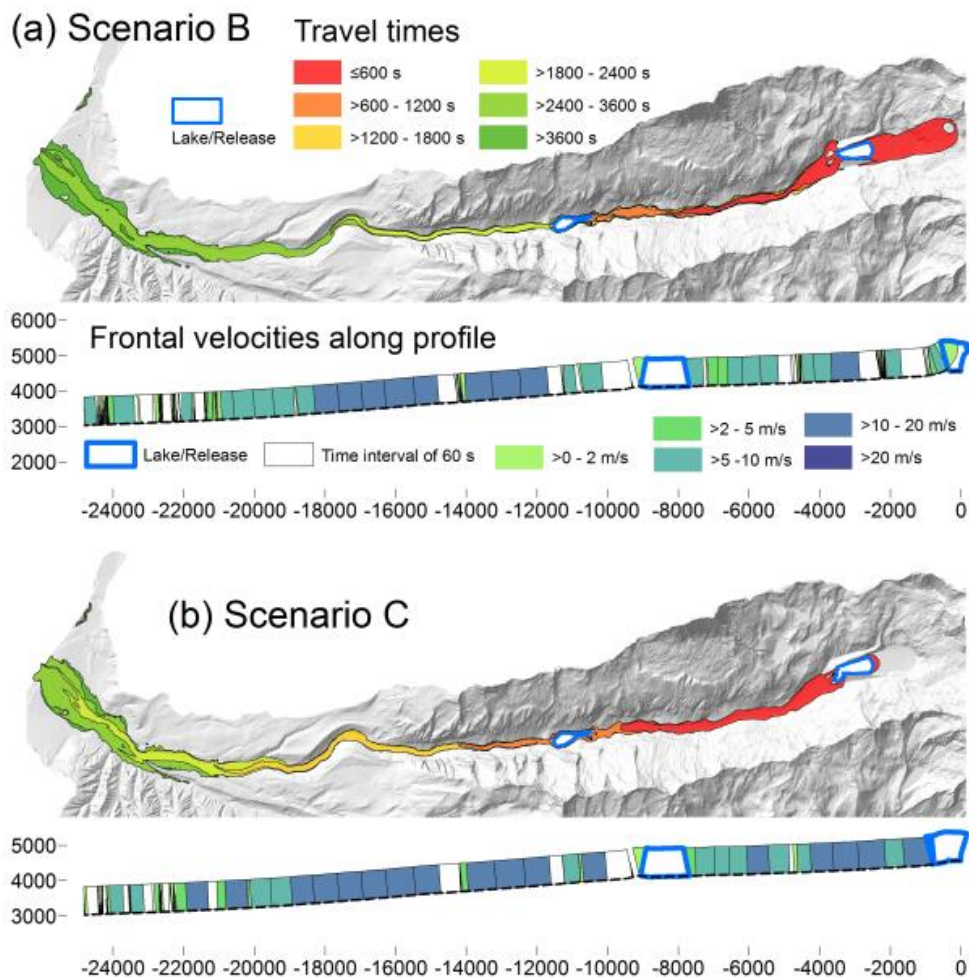
(b) Lake Jircacocha - Scenario B



(c) Lake Jircacocha - Scenario C



841
 842 Fig. 11. Simulated versus reconstructed entrainment patterns for the scenarios B and C. The total entrained height and
 843 the difference between simulated and reconstructed entrainment (error) are shown. (a) Lake Palcacocha, Scenario B.
 844 (b) Lake Jircacocha, Scenario B. (c) Lake Jircacocha, Scenario C.
 845



846
847
848
849

Fig. 12. Travel times and frontal velocities for the scenarios (a) B and (b) C. Note that the legend of (a) also applies to (b). Void fields in the profile graph refer to areas without clearly defined flow front.